What's new?

While genetic abnormalities are well studied in human cancers, epigenetic changes, especially in the early stages of carcinogenesis, remain largely unknown. Here, the authors perform a genome-wide analysis focusing on DNA methylation profiles in "normal" lung tissue adjacent to lung adenocarcinomas. Using single-CpG-resolution Infinium assays, they identify distinct DNA methylation profiles clustering with specific risk factors such as cigarette smoking, inflammation and chronic obstructive pulmonary disease. The authors speculate that these epigenetic profiles detected in the neighboring cells may influence the aggressiveness of tumors developing in individual patients and may thus help predict disease outcome.

mutations, G:C to T:A transversions and A:T to G:C transitions at CpG sites are characteristic of smoking-related lung cancers, whereas G:C to A:T transitions at non-CpG sites are associated with lung cancers in individuals who have never smoked. However, the molecular changes responsible for the development of LADCs in both smokers and nonsmokers, especially at the very early stages, are not yet fully understood.

As well as genetic abnormalities, epigenetic changes have been described in human cancers,[3] one of the most consistent being DNA methylation alterations. In LADCs, silencing of the *RASSF1A, CDKN2A, RARβ, MGMT, APC, DAPK, FHIT* and *CDH13* genes due to DNA hypermethylation around their promoter regions has been frequently reported.[4] Moreover, in various organs, DNA methylation alterations are characteristically observed even at the precancerous stage[5–7]: we and other groups have reported aberrant DNA methylation of specific genes or chromosomal loci in non-cancerous lung tissue from LADC patients, or in lung tissue from cancer-free smokers.[4,8,9] DNA methylation alterations of tumor-related genes have been reported in airway epithelial cells from smokers.[8,10,11] Recently, methylome analysis using single-CpG-resolution Infinium assay has been introduced.[12] Although studies of lung cancers using the Infinium assay by Selamat *et al.*[13] and Lockwood *et al.*[14] did not focus on non-cancerous lung tissue obtained from the same patients, our previous study revealed that alterations of DNA methylation status in adjacent lung tissue are not nonsensical, but in fact create alterations in the expression of mRNAs for specific genes in cancerous tissue developing in the same individual patients.[15]

It is known that DNA methylation profiles at the precancerous stage are determined by carcinogenetic factors. For examples, distinct DNA methylation profiles at the chronic hepatitis or liver cirrhosis stage as a precancerous condition for hepatocellular carcinoma[16,17] or those in the stomach mucosa harboring *Helicobacter pylori* infection as a precancerous condition for stomach adenocarcinoma have been reported.[18] In this study, to further understand the significance of DNA methylation alterations during lung carcinogenesis, we examined correlations between epigenetic clustering of patients with LADCs based on DNA methylation profiles in adjacent lung tissue and carcinogenetic factors such as cigarette smoking and chronic obstructive lung disease (COPD).

Material and Methods

Patients and tissue samples

As a learning cohort, 139 paired samples of non-cancerous lung tissue (N) and the corresponding tumorous tissue (T) were obtained from patients with primary LADCs who underwent lung resection at the National Cancer Center Hospital, Japan, between December 2000 and May 2008. None of these patients had received any preoperative treatment. Sixty-nine patients were males and seventy were females with a median age of 60 years (range, 30–76 years). Clinicopathological parameters in the learning cohort are summarized in Supporting Information Table S1. Pleural anthracosis, which mainly reflects the cumulative effects of smoking history, was evaluated macroscopically according to the criteria described previously.[19] Presence or absence of emphysematous change, respiratory bronchiolitis, interstitial fibrosis[20,21] and atypical adenomatous hyperplasia (AAH, a precancerous lesion for LADC)[22,23] was evaluated microscopically on the basis of the criteria described previously. Histological diagnosis and grading were based on the 2004 World Health Organization classification.[24] When, within a tumor, black dusty material[25] is seen to have accumulated in foci of active fibroblast proliferation, reflecting active cancer–stromal interaction associated with a poorer outcome in LADC patients,[26] the tumor is considered to be tumor anthracosis-positive (Supporting Information Fig. S1). All the tumors were classified according to the pathological tumor-node-metastasis (TNM) classification.[27] Recurrence was diagnosed by clinicians on the basis of physical examination and imaging modalities such as computed tomography, magnetic resonance imaging, scintigraphy or positron-emission tomography, and sometimes confirmed histopathologically by biopsy. A proportion of this cohort had also been included in our previous study focusing on recurrence-related genes.[15]

DNA methylation profiles of the 139 N samples and 139 T samples were compared with previously reported DNA methylation profiles of 36 samples of normal lung tissue (C) obtained from specimens surgically resected from 36 patients without any primary lung tumors.[15] Briefly, 22 of these patients were males and 14 were females, with a median age of 63 years (range, 27–83 years). Thirty-five had undergone lung resection for metastatic lesions from primary cancers of the colon, rectum, kidney, urinary bladder, thyroid, breast, pancreas, ampulla of Vater and salivary gland, osteosarcoma, synovial sarcoma, leiomyosarcoma, rhabdomyosarcoma,

liposarcoma, dermatofibrosarcoma and myxofibrosarcoma. The remaining one patient had undergone chest wall resection for lipoma with removal of adjacent lung tissue.

As a validation cohort, 50 paired samples of N and the corresponding T were obtained from patients with primary LADCs who underwent lung resection at the National Cancer Center Hospital, Japan, between December 1997 and May 2000. None of these patients had received any preoperative treatment. Thirty-three patients were males and seventeen were females with a median age of 63 years (range, 40–81 years). Clinicopathological parameters in the validation cohort are summarized in Supporting Information Table S1.

Tissue specimens were provided by the National Cancer Center Biobank, Japan. This study was approved by the Ethics Committee of the National Cancer Center, Japan, and was performed in accordance with the Declaration of Helsinki. All patients included in this study provided written informed consent.

Infinium assay

Genomic DNA was extracted from all tissue samples using a QIAamp DNA Mini kit (Qiagen, Valencia, CA). Five-hundred-nanogram aliquots of DNA were subjected to bisulfite conversion using an EZ DNA Methylation-Gold Kit (Zymo Research, Irvine, CA). Subsequently, DNA methylation status at 27,578 CpG loci was examined at single-CpG resolution using the Infinium HumanMethylation27 Bead Array (Illumina, San Diego, CA). This array contains CpG sites located mainly within the proximal promoter regions of the transcription start sites of 14,475 consensus coding sequences in the National Center for Biotechnology Information Database. An Evo robot (Tecan, Männedorf, Switzerland) was used for automated sample processing. After whole-genome amplification and hybridization, the specifically hybridized DNA was fluorescence-labeled by a single-base extension reaction and detected using a BeadScan reader (Illumina) in accordance with the manufacturer's protocols. The data were then assembled using GenomeStudio methylation software (Illumina). At each CpG site, the ratio of the fluorescence signal was measured using a methylated probe relative to the sum of the methylated and unmethylated probes, that is, the so-called β-value, which ranges from 0.00 to 1.00, reflecting the methylation level of an individual CpG site.

The reliability of DNA methylation levels (β-values) determined by Infinium assay has been verified in our previous studies.[7,15] In addition, DNA methylation levels of the representative genes (*NUPR1, EVI2B, CASP8* and *KRTAP11-1* genes) based on the Infinium assay in representative samples included in this study were verified using the quantitative pyrosequencing method (Supporting Information Fig. S2), thus confirming the reliability of the Infinium assay. Moreover, we compared the DNA methylation levels of 545 representative Infinium probes, whose β values were unrelated to the clinicopathological parameters of the tumors or patient outcome (recurrence or death), between all samples in the learning cohort (obtained between December 2000 and May 2008) and the validation cohort (obtained between December 1997 and May 2000). No significant differences in DNA methylation levels between the learning and validation cohorts were observed in any of the 545 probes examined (Supporting Information Fig. S3). Supporting Information Figure S3 clearly indicates the excellent concordance of DNA methylation status between the two cohorts ($r = 1.000$, $p < 2.20 \times 10^{-16}$), confirming that the epigenetic changes did not degrade over time.

Statistics

In the Infinium assay, all CpG sites on chromosomes X and Y were excluded, to avoid any gender-specific methylation bias. In addition, the call proportions (p-value of <0.01 for detection of signals above the background) for 39 probes (shown in Supporting Information Table S2) in 36 C samples, 139 N samples and 139 corresponding T samples in the learning cohort were less than 90%. As such a low proportion may be attributable to polymorphism at the probe CpG sites, these 39 probes were excluded from the present assay, leaving a final total of 26,447 autosomal CpG sites.

Infinium probes showing significant differences in DNA methylation levels between the 36 C samples and 139 N samples in the learning cohort were identified by the Welch's t-test. Ordered differences from 36 C to 139 N, and then to 139 T samples themselves in the learning cohort were examined by the Jonckheere–Terpstra trend test. A false discovery rate (FDR) of $q = 0.01$ was considered significant. Unsupervised hierarchical clustering (Euclidean distance, Ward method) based on DNA methylation levels of the 139 N samples in the learning cohort was performed. Correlations between clusters of patients and clinicopathological parameters were examined using Kruskal–Wallis test, Fisher's exact test and Kruskal–Wallis exact test at a significance level of $p < 0.05$. Survival curves of patients belonging to each cluster were calculated by the Kaplan–Meier method, and the differences were compared by the Log-rank test. The hallmark genes discriminating the clusters were identified by Welch's t-test. Correlations between DNA methylation levels of such hallmark genes in N samples and clinicopathological parameters of patients in the validation cohort were examined using Welch's t-test and ANOVA test at a significance level of $p < 0.05$. All statistical analyses were performed using programming language R.

Results

DNA methylation alterations during lung carcinogenesis

(*i*) Welch's t-test revealed that DNA methylation levels on the 3,778 probes were already altered in N samples in the learning cohort relative to those in C samples (FDR, $q = 0.01$, Table 1A). (*ii*) The Jonckheere–Terpstra trend test revealed ordered differences in the DNA methylation level from the 39 C samples to the 139 N samples, and then to the 139 T samples themselves in the learning cohort on the 12,368 probes (FDR, $q = 0.01$, Table 1B). (*iii*) Among the probes, 1,928 satisfied

Table 1. DNA methylation alterations during lung carcinogenesis

The number of probes showing DNA hypermethylation and DNA hypomethylation	
(A) The probes on which DNA methylation levels were altered in 139 samples of non-cancerous lung tissue (N) obtained from patients with lung adenocarcinomas (LADCs) in the learning cohort relative to those in 39 samples of normal lung tissue (C) obtained from patients without any primary lung tumors. (Welch's *t*-test, False discovery rate [FDR] $q = 0.01$)	
DNA hypermethylation ($\beta_C < \beta_N$)	1,526
DNA hypomethylation ($\beta_C > \beta_N$)	2,252
Total	3,778
(B) The probes on which DNA methylation levels showed ordered differences from 39 C samples to 139 N samples, and then to 139 tumorous tissue (T) samples in the learning cohort. (Jonckheere–Terpstra trend test, FDR $q = 0.01$)	
DNA hypermethylation ($\beta_C < \beta_N < \beta_T$, $\beta_C < \beta_N \fallingdotseq \beta_T$ or $\beta_C \fallingdotseq \beta_N < \beta_T$)	6,460
DNA hypomethylation ($\beta_C > \beta_N > \beta_T$, $\beta_C > \beta_N \fallingdotseq \beta_T$ or $\beta_C \fallingdotseq \beta_N > \beta_T$)	5,908
Total	12,368
(C) The probes satisfying both of the above criteria (A) and (B): DNA methylation alterations on these probes occurred even in N samples relative to C samples, and such DNA methylation alterations were inherited by, or strengthened in, T samples.	
DNA hypermethylation ($\beta_C < \beta_N < \beta_T$ or $\beta_C < \beta_N \fallingdotseq \beta_T$)	484
DNA hypomethylation ($\beta_C > \beta_N > \beta_T$ or $\beta_C > \beta_N \fallingdotseq \beta_T$)	1,444
Total	1,928

the above criteria (*i*) and (*ii*): DNA methylation alterations on the 1,928 probes occurred even in N samples relative to C samples, and such DNA methylation alterations were inherited by, or strengthened in, the T samples (Table 1C).

Epigenetic clustering of LADCs based on DNA methylation profiles in N samples

As DNA methylation alterations already occurred in Ns, unsupervised hierarchical clustering using DNA methylation levels in N samples (β_N) on all 26,447 probes was performed in 139 patients with LADCs in the learning cohort. Such clustering based on DNA methylation profiles in N samples subclustered 139 patients in the learning cohort into Cluster I ($n = 32$), Cluster II ($n = 35$) and Cluster III ($n = 72$, Fig. 1*a*). The clinicopathological parameters of the patients in these clusters are summarized in Table 2.

Most of the patients in Cluster I were heavy smokers (median number of cigarettes smoked per day × year index: 810) and frequently showed severe pleural anthracosis, which mainly reflects the cumulative effects of smoking.[19] With regard to the non-cancerous lung tissue, patients belonging to Cluster I frequently showed histological findings compatible with emphysema, respiratory bronchiolitis and interstitial fibrosis, and they frequently suffered from obstructive ventilation impairment (Table 2). In Cluster I, LADCs with a large diameter, a progressed T stage, a high histological grade and frequent pleural invasion were accumulated (Table 2). In addition, tumor anthracosis reflecting active cancer–stromal interaction[26] was frequent in Cluster I (Table 2). These data indicated that LADCs in Cluster I were locally invasive tumors.

Most of the patients in Cluster II were non-smokers (median number of cigarettes smoked per day × year index: 0) and less frequently showed emphysematous changes in their adjacent lung tissue (Table 2). The correlation between epigenetic clustering of LADCs and patient age and sex may be attributable to the fact that younger female non-smokers[28] were accumulated in Cluster II. LADCs in Cluster II showed less aggressive clinicopathological features (Table 2).

Most of the patients in Cluster III were light smokers and tended to have a lower incidence of emphysematous changes in their adjacent lung tissue (Table 2). LADCs in Cluster III frequently showed lymphatic vessel invasion, blood vessel invasion, high N stage and high TNM stage (Table 2), indicating that they were the most aggressive tumors.

Figure 1*b* shows the Kaplan–Meier survival curves of patients belonging to Clusters I, II and III. The period covered ranged from 196 to 3,957 days (mean, 1,634 days). The cancer-free and overall survival rates of patients in Cluster III were significantly lower than those of patients in Cluster II ($p = 1.24 \times 10^{-4}$ and $p = 1.58 \times 10^{-2}$, respectively, Fig. 1*b*).

DNA methylation profiles of N samples belonging to each cluster in the learning cohort

Scattergrams of average DNA methylation levels in N samples ($_{average}\beta_N$) of patients belonging to Clusters I, II and III and average DNA methylation levels in C samples ($_{average}\beta_C$) for all 26,447 probes are shown in Figure 2. In Cluster I, DNA methylation levels on probes normally showing a low or medium degree of DNA methylation ($_{average}\ \beta_C < 0.6$) were elevated in N samples relative to C samples, and DNA methylation levels on probes normally showing a high or medium degree of DNA methylation ($_{average}\ \beta_C > 0.3$) were reduced in N samples relative to C samples (Fig. 2*a*). In Cluster II, DNA methylation levels on probes normally showing a low degree of DNA methylation ($_{average}\ \beta_C < 0.2$) were elevated in N samples relative to C samples, and DNA methylation levels on probes normally showing a high degree of DNA methylation ($_{average}\ \beta_C > 0.7$) were reduced in N

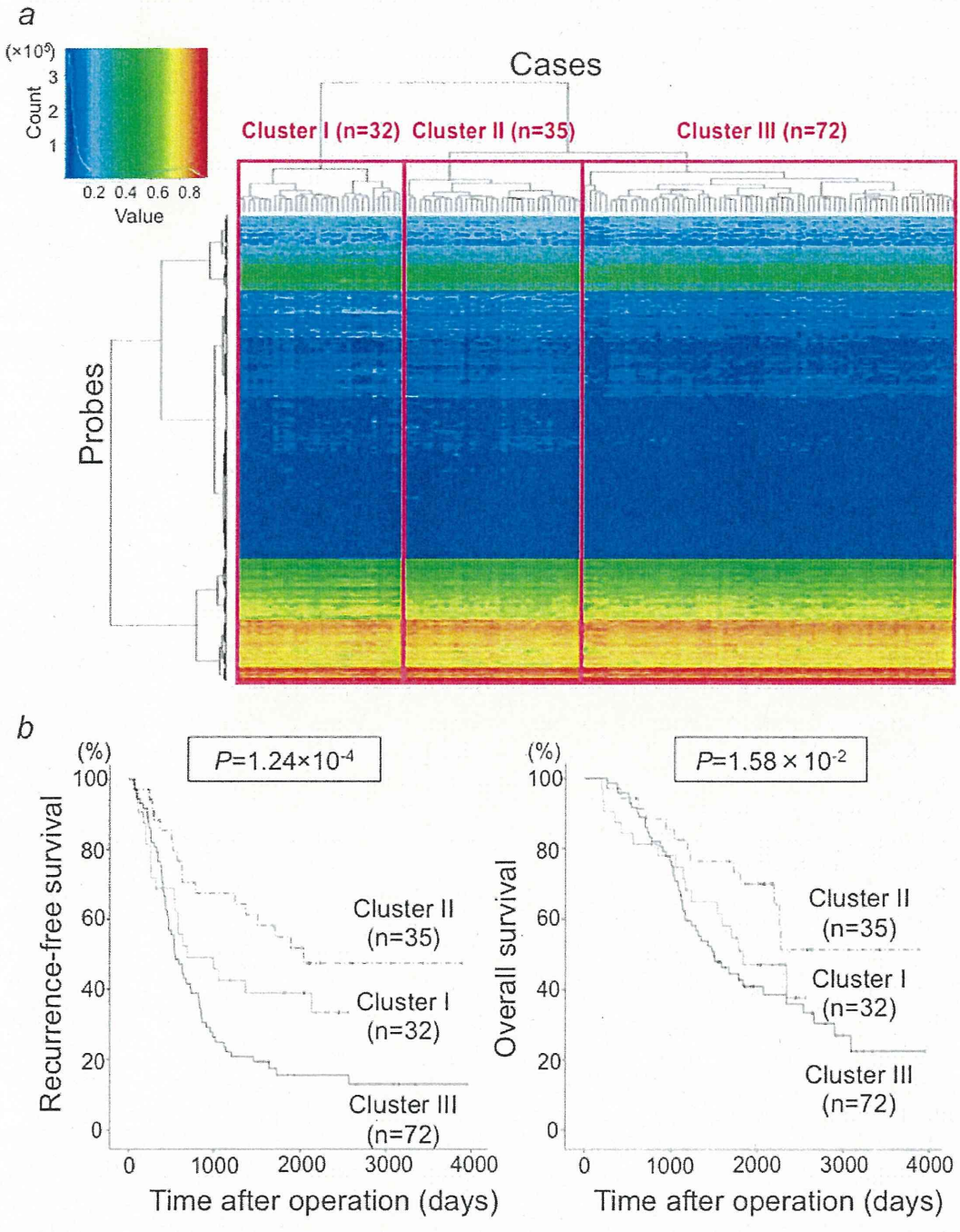

Figure 1. (*a*) Unsupervised hierarchical clustering (Euclidean distance, Ward method) using DNA methylation levels on all 26,447 probes in samples of non-cancerous lung tissue (N) from 139 patients with lung adenocarcinomas in the learning cohort. Based on DNA methylation status in adjacent lung tissue, 139 patients were subclustered into Cluster I ($n = 32$), Cluster II ($n = 35$) and Cluster III ($n = 72$). Correlations between this epigenetic clustering and clinicopathological parameters of the patients are summarized in Table 2. (*b*) Kaplan–Meier survival curves of patients belonging to Clusters I, II and III. The period covered ranged from 196 to 3,957 days (mean, 1,634 days). The cancer-free ($p = 1.24 \times 10^{-4}$) and overall ($p = 1.58 \times 10^{-2}$) survival rates of patients in Cluster III were significantly lower than those of patients in Cluster II (log-rank test).

Table 2. Correlation between epigenetic clustering of patients with lung adenocarcinomas based on DNA methylation profiles in adjacent lung tissue and clinicopathological parameters

Clinicopathological parameters		Cluster I (n = 32)	Cluster II (n = 35)	Cluster III (n = 72)	P^1
Patients	Age (year)				
	Median	64	57	60	2.03×10^{-2} [2]
	Interquartile range	59–68	54–62	53–64	
	Sex				
	Male	24	11	34	1.35×10^{-3} [3]
	Female	8	24	38	
	Smoking history (number of cigarettes smoked per day × year index)				
	Median	810	0	0	8.80×10^{-6} [2]
	Interquartile range	195–1,113	0–140	0–635	
Adjacent lung tissue					
	Pleural anthracosis				
	G1	13	24	48	2.46×10^{-2} [4]
	G2-3	19	11	24	
	Emphysematic change				
	Negative	8	24	46	2.50×10^{-4} [4]
	Positive	24	11	26	
	Respiratory bronchiolitis				
	Negative	2	14	10	2.80×10^{-3} [4]
	Positive	22	21	58	
	Interstitial fibrosis				
	Negative	24	35	68	5.72×10^{-4} [4]
	Positive	8	0	4	
	Obstructive ventilation impairment				
	Forced expiratory volume in 1 sec (FEV_1): forced vital capacity (FVC) $\geq$0.70	24	34	65	9.86×10^{-3} [4]
	FEV_1:FVC <0.70				
	FEV_1 $\geq$80% of predicted value	4	1	6	
	FEV_1 <80% but $\geq$50% of predicted value	4	0	1	
	Atypical adenomatous hyperplasia				
	Absence	30	30	65	5.72×10^{-1} [4]
	Presence	2	5	7	
Lung adenocarcinomas					
	Tumor diameter (cm)				
	Median	3.4	2.3	3.1	1.64×10^{-4} [4]
	Interquartile range	2.5–4.9	2.1–2.9	2.5–4.5	
	Tumor stage				
	T1a-T1b	6	19	19	1.60×10^{-4} [4]
	T2a-T2b	12	14	39	
	T3-4	14	2	14	
	Histological grades				
	G1	8	20	26	2.37×10^{-3} [4]
	G2	11	12	34	
	G3	13	3	12	

Table 2. Correlation between epigenetic clustering of patients with lung adenocarcinomas based on DNA methylation profiles in adjacent lung tissue and clinicopathological parameters (Continued)

Clinicopathological parameters	Cluster I (n = 32)	Cluster II (n = 35)	Cluster III (n = 72)	P[1]
Tumor anthracosis				
Negative	6	20	39	1.70×10^{-3} [4]
Positive	25	15	33	
Pleural invasion				
Negative	12	22	35	9.62×10^{-3} [4]
Invasion to the visceral pleura beyond the elastic fiber	6	9	17	
Invasion to the surface of the visceral pleura	4	4	15	
Invation to the parietal pleura	10	0	5	
Lymphatic vessel invasion				
Negative	9	18	16	8.54×10^{-3} [4]
Positive	23	17	56	
Blood vessel invasion				
Negative	7	18	15	3.02×10^{-3} [4]
Positive	25	17	57	
Nodal status				
N0	17	26	25	8.72×10^{-5} [4]
N1	10	6	18	
N2-3	5	3	29	
Metastatic status				
M0	31	34	66	4.40×10^{-1} [4]
M1a-1b	1	1	1	
Pathological Tumor-Node-Metastasis stage				
IA-IB	5	24	18	4.36×10^{-6} [4]
IIA-IIB	21	7	19	
IIIA-IV	6	4	35	

[1]*P*values of <0.05 are underlined.
[2]Kruskal-Wallis test.
[3]Fisher's exact test.
[4]Kruskal-Wallis exact test.

samples relative to C samples (Fig. 2*b*). In Cluster III, DNA methylation levels on probes normally showing a high or medium degree of DNA methylation ($_{average}\ \beta_C > 0.3$) were reduced in N samples relative to C samples (Fig. 2*c*).

Hallmark CpG sites for each cluster in the learning cohort

One hundred sixteen CpG sites were identified as hallmarks of the DNA methylation profile (Fig. 2*a*) of N samples belonging to Cluster I: on these 116 CpG sites, the average β_{N-C} values in Cluster I were significantly different from those in Clusters II and III (Welch's *t*-test, $p < 1 \times 10^{-3}$) and the average β_{N-C} value in Cluster I was 0.1 or more higher or lower than those in Clusters II and III (Table 3A and Supporting Information Table S3). One CpG site was identified as a hallmark for the DNA methylation profile (Fig. 2*b*) of N samples belonging to Cluster II: on the CpG site, the average β_{N-C} value in Cluster II was significantly different from that in Clusters I and III (Welch's *t*-test, $p < 1 \times 10^{-3}$) and the average β_{N-C} value in Cluster II was 0.1 or more higher than those in Clusters I and III (Table 3B). Four CpG sites were identified as a hallmark for the DNA methylation profile (Fig. 2*c*) of N samples belonging to Cluster III: on the four CpG sites, average β_{N-C} values in Cluster III were significantly different from those in Clusters I and II (Welch's *t*-test, $p < 1 \times 10^{-3}$) and average β_{N-C} values in Cluster III were 0.1 or more higher or lower than those in Clusters I and II (Table 3C). In 119 of the 120 CpG sites in Table 3 or Supporting Information Table S3, which were identified based on the DNA methylation profiles in N samples, stepwise DNA methylation alterations from C to N, and then to T samples were revealed by Jonckheere–Terpstra trend test (Table 3 and Supporting Information Table S3).

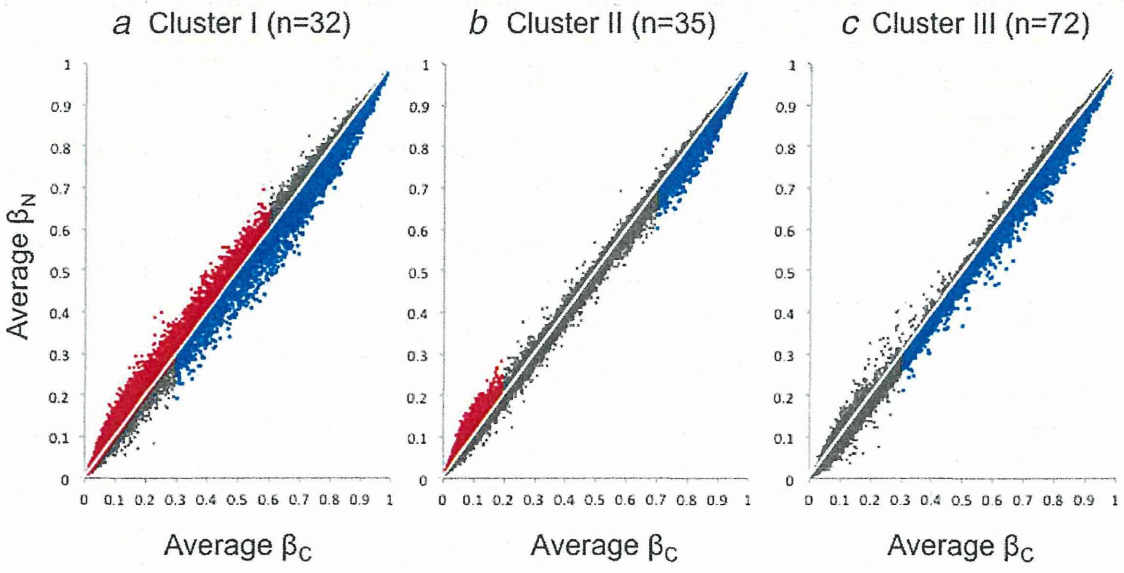

Figure 2. Distribution of average DNA methylation levels on all 26,447 probes of non-cancerous lung tissue (N) samples obtained from patients with lung adenocarcinomas belonging to Clusters I (*a*), II (*b*) and III (*c*) and 36 samples of normal lung tissue (C) obtained from patients without any primary lung tumors. (*a*) In Cluster I, DNA methylation levels on probes normally showing a lower or medium degree of DNA methylation ($_{average}\beta_C < 0.6$, red) were elevated in N samples relative to C samples, and DNA methylation levels on probes normally showing a higher or medium degree of DNA methylation ($_{average}\ \beta_C > 0.3$, blue) were reduced in N samples relative to C samples. (*b*) In Cluster II, DNA methylation levels on probes normally showing a lower degree of DNA methylation ($_{average}\ \beta_C < 0.2$,red) were elevated in N samples relative to C samples, and DNA methylation levels on probes normally showing a higher degree of DNA methylation ($_{average}\ \beta_C > 0.7$,blue) were reduced in N samples relative to C samples. (*c*) In Cluster III, DNA methylation levels on probes normally showing a higher or medium degree of DNA methylation ($_{average}\ \beta_C > 0.3$,blue) were reduced in N samples relative to C samples.

DNA methylation profiles in the validation cohort

The correlations between the DNA methylation status of hallmark CpG sites for Clusters I, II and III in N samples and clinicopathological parameters of patients in the validation cohort were examined. DNA methylation levels on 17 and 2 hallmark CpG sites for Cluster I were significantly correlated with pleural anthracosis and pulmonary emphysema in the adjacent lung tissue in the validation cohort, respectively (Table 4A), whereas hallmark CpG sites for Clusters II and III never showed such a correlation. In addition, in the validation cohort, DNA methylation levels on 18 hallmark CpG sites for Cluster I were significantly correlated with the presence of AAH, a precancerous lesion for LADCs, in the adjacent lung tissue (Table 4A), even though the correlation between the presence of AAH and epigenetic clustering did not reach statistically significant levels (Table 2). DNA methylation levels on 13 hallmark CpG sites for Cluster I were significantly correlated with tumor anthracosis in LADCs in the validation cohort (Table 4A), whereas hallmark genes for Clusters II and III never showed such a correlation. Hallmark genes for Cluster I showing such correlations with pleural anthracosis, emphysema, presence of AAH or tumor anthracosis are described in Table 3A, and hallmark genes not showing such correlations are described in Supporting Information Table S3.

Hallmark gene *ABCC12* was shared between Clusters II and III. The DNA methylation level of *ABCC12* was significantly correlated with N stage and TNM stage in the validation cohort (Table 4B). In the learning cohort, the DNA methylation level of the *ABCC12* gene was high in Cluster II showing low N and TNM stages, and that of the *ABCC12* gene was low in Cluster III showing high N and TNM stages. Therefore, it is feasible that the DNA methylation level of the *ABCC12* gene was significantly higher in patients showing lower N and TNM stages in the validation cohort (Table 4B). DNA methylation levels of two of the three remaining hallmark genes (three hallmark genes other than *ABCC12*) for Cluster III were significantly correlated with lymph vessel invasion in LADCs in the validation cohort, and the DNA methylation levels of all three remaining hallmark genes for Cluster III were significantly correlated with high N and TNM stages (Table 4B). Taken together, correlations between DNA methylation profiles in N samples and clinicopathological characteristics in the adjacent lung tissue or LADCs in the learning cohort were reproduced in the validation cohort.

Discussion

In this study, we focused on DNA methylation profiles in the adjacent non-cancerous lung tissue obtained from patients with LADCs and analyzed the results of methylome analysis of lung tissue samples including 189 N samples at single-CpG resolution. DNA methylation alterations occurred even in N samples relative to C samples, and were inherited by, or

Table 3. Genes for which DNA methylation levels were hallmarks for Clusters I, II and III in the learning cohort

(A) Hallmark genes for Cluster I

Target ID [1]	Chrom[2]	Position[3]	Gene symbol	DNA methylation level in non-cancerous lung tissue (N) samples[4] (mean ± SD)			*p*-Value of Welch's *t*-test (I *vs.* II and III)[5]	Δβ (I-II and III)[6]	*p*-Value of Jonckheere–Terpstra trend test in I[7]
				Cluster I	Cluster II	Cluster III			
cg20249919	15	102,029,706	*PCSK6*	0.091 ± 0.188	−0.047 ± 0.109	−0.070 ± 0.125	9.28×10^{-5}	0.153	6.51×10^{-4} (Hyper)
cg23349790	1	18,434,576	*IGSF21*	0.114 ± 0.133	−0.011 ± 0.111	−0.032 ± 0.108	2.41×10^{-6}	0.139	4.43×10^{-9} (Hyper)
cg22285621	11	67,071,322	*SSH3*	0.103 ± 0.116	−0.031 ± 0.075	−0.033 ± 0.082	2.32×10^{-7}	0.136	3.69×10^{-7} (Hyper)
cg15433631	5	2,751,541	*IRX2*	0.123 ± 0.083	−0.007 ± 0.073	0.000 ± 0.070	8.88×10^{-10}	0.125	6.60×10^{-8} (Hyper)
cg21949305	22	24,828,655	ADORA2A, CYTSA	0.109 ± 0.053	−0.015 ± 0.040	−0.010 ± 0.052	2.91×10^{-15}	0.121	0 (Hyper)
cg10942056	1	223,101,848	*DISP1*	0.095 ± 0.059	−0.027 ± 0.039	−0.026 ± 0.048	1.59×10^{-13}	0.121	4.05×10^{-13} (Hyper)
cg15149645	16	28,550,619	NUPR1	0.090 ± 0.067	−0.023 ± 0.044	−0.033 ± 0.058	7.39×10^{-12}	0.12	1.36×10^{-12} (Hyper)
cg06954481	2	237,076,497	*GBX2*	0.096 ± 0.111	−0.012 ± 0.051	−0.029 ± 0.052	1.02×10^{-6}	0.119	1.25×10^{-7} (Hyper)
cg21250978	7	106,684,541	*PRKAR2B*	0.088 ± 0.060	−0.026 ± 0.044	−0.031 ± 0.056	4.25×10^{-13}	0.118	6.13×10^{-9} (Hyper)
cg22418909	8	41,166,738	SFRP1	0.091 ± 0.082	−0.023 ± 0.055	−0.029 ± 0.052	2.38×10^{-9}	0.118	1.22×10^{-10} (Hyper)
cg26200585	19	40,919,245	*PRX*	0.099 ± 0.059	−0.019 ± 0.040	−0.019 ± 0.054	2.44×10^{-13}	0.118	0 (Hyper)
cg24396745	15	73,660,614	*HCN4*	0.096 ± 0.098	−0.022 ± 0.073	−0.015 ± 0.089	3.31×10^{-7}	0.114	1.96×10^{-8} (Hyper)
cg04330449	5	134,871,166	*NEUROG1*	0.098 ± 0.080	−0.001 ± 0.061	−0.019 ± 0.051	5.89×10^{-9}	0.111	1.08×10^{-13} (Hyper)
cg19589427	1	173,019,720	*TNFSF18*	0.076 ± 0.073	−0.036 ± 0.039	−0.032 ± 0.051	9.08×10^{-10}	0.11	7.78×10^{-10} (Hyper)
cg16731240	19	52,391,250	*ZNF577*	0.090 ± 0.105	−0.015 ± 0.072	−0.022 ± 0.061	1.87×10^{-6}	0.11	0 (Hyper)
cg03544320	4	5,894,691	*CRMP1*	0.088 ± 0.108	−0.016 ± 0.105	−0.022 ± 0.101	7.22×10^{-6}	0.108	1.61×10^{-10} (Hyper)
cg12864235	5	27,038,782	*CDH9*	0.092 ± 0.059	−0.011 ± 0.037	−0.018 ± 0.040	3.56×10^{-12}	0.108	2.37×10^{-13} (Hyper)
cg15898840	7	45,960,834	*IGFBP3*	0.102 ± 0.095	−0.001 ± 0.052	−0.008 ± 0.058	4.67×10^{-7}	0.107	2.02×10^{-8} (Hyper)
cg08044694	19	15,391,927	BRD4	0.068 ± 0.072	−0.029 ± 0.034	−0.044 ± 0.042	1.55×10^{-9}	0.107	1.76×10^{-8} (Hyper)
cg03734874	14	105,071,382	*TMEM179*	0.099 ± 0.068	0.001 ± 0.056	−0.012 ± 0.055	3.06×10^{-10}	0.106	4.39×10^{-13} (Hyper)
cg10599444	14	23,305,941	*MMP14*	0.064 ± 0.065	−0.039 ± 0.040	−0.044 ± 0.056	8.35×10^{-11}	0.106	7.42×10^{-7} (Hyper)
cg24133115	6	166,075,520	*PDE10A*	0.096 ± 0.071	−0.007 ± 0.054	−0.010 ± 0.046	1.50×10^{-9}	0.105	9.66×10^{-10} (Hyper)
cg12594641	2	150,187,223	*LYPD6*	0.111 ± 0.064	0.011 ± 0.071	0.004 ± 0.061	1.05×10^{-10}	0.105	6.56×10^{-7} (Hyper)
cg05724065	7	56,160,528	PHKG1	0.082 ± 0.053	−0.017 ± 0.029	−0.026 ± 0.044	3.01×10^{-13}	0.105	4.43×10^{-11} (Hyper)
cg19466563	4	88,450,506	SPARCL1	0.081 ± 0.053	−0.018 ± 0.027	−0.027 ± 0.042	4.93×10^{-13}	0.104	0 (Hyper)
cg24433189	16	1,128,689	SSTR5	0.092 ± 0.056	−0.005 ± 0.052	−0.015 ± 0.064	2.58×10^{-12}	0.104	9.78×10^{-9} (Hyper)
cg24453664	11	33,758,413	CD59	0.069 ± 0.066	−0.031 ± 0.033	−0.036 ± 0.046	3.23×10^{-10}	0.103	9.78×10^{-9} (Hyper)

Table 3. Genes for which DNA methylation levels were hallmarks for Clusters I, II and III in the learning cohort (Continued)

(A) Hallmark genes for Cluster I

Target ID [1]	Chrom[2]	Position[3]	Gene symbol	DNA methylation level in non-cancerous lung tissue (N) samples[4] (mean ± SD)			*p*-Value of Welch's *t*-test (I *vs.* II and III)[5]	Δβ (I-II and III)[6]	*p*-Value of Jonckheere–Terpstra trend test in I[7]
				Cluster I	Cluster II	Cluster III			
cg26609631	13	28,366,814	GSX1	0.077 ± 0.081	−0.025 ± 0.063	−0.026 ± 0.057	4.72×10^{-8}	0.103	1.73×10^{-11} (Hyper)
cg10604646	1	163,172,649	RGS5	0.086 ± 0.041	−0.029 ± 0.059	−0.009 ± 0.060	4.09×10^{-17}	0.102	2.68×10^{-14} (Hyper)
cg03355526	5	178,368,415	ZNF454	0.073 ± 0.070	−0.024 ± 0.043	−0.030 ± 0.061	2.48×10^{-9}	0.101	9.13×10^{-13} (Hyper)
cg27096144	5	174,151,779	MSX2	0.074 ± 0.078	−0.020 ± 0.054	−0.030 ± 0.056	3.60×10^{-8}	0.101	2.11×10^{-7} (Hyper)
cg15520279	2	176,995,088	HOXD8	0.095 ± 0.083	0.008 ± 0.048	−0.013 ± 0.046	1.06×10^{-7}	0.1	1.30×10^{-13} (Hyper)
cg11733245	10	6,104,312	IL2RA	−0.112 ± 0.066	−0.001 ± 0.028	−0.016 ± 0.050	5.58×10^{-10}	−0.101	8.03×10^{-13} (Hypo)
cg22325572	1	111,416,181	CD53	−0.102 ± 0.062	0.013 ± 0.035	−0.007 ± 0.048	9.63×10^{-11}	−0.102	3.52×10^{-12} (Hypo)
cg15691199	14	23,589,419	CEBPE	−0.102 ± 0.061	0.006 ± 0.033	−0.003 ± 0.052	4.72×10^{-11}	−0.102	1.33×10^{-9} (Hypo)
cg16927606	19	36,233,324	U2AF1L4	−0.086 ± 0.048	0.013 ± 0.028	0.018 ± 0.044	3.10×10^{-14}	−0.103	1.79×10^{-8} (Hypo)
cg16240480	1	236,557,473	EDARADD	−0.128 ± 0.064	−0.005 ± 0.039	−0.030 ± 0.049	7.69×10^{-11}	−0.106	1.59×10^{-9} (Hypo)
cg05596756	12	47,610,220	FAM113B	−0.102 ± 0.060	0.009 ± 0.029	0.016 ± 0.047	8.28×10^{-13}	−0.116	1.53×10^{-10} (Hypo)
cg08040471	17	80,407,779	C17orf62	−0.116 ± 0.067	0.008 ± 0.036	0.004 ± 0.047	6.99×10^{-12}	−0.121	5.63×10^{-11} (Hypo)
cg20622019	20	43,279,793	ADA	−0.108 ± 0.072	0.020 ± 0.043	0.012 ± 0.042	3.92×10^{-11}	−0.123	1.56×10^{-13} (Hypo)
cg05109049	17	29,641,333	EVI2B	−0.141 ± 0.081	0.007 ± 0.050	−0.020 ± 0.063	1.98×10^{-10}	−0.13	2.31×10^{-14} (Hypo)
cg07973967	17	62,009,607	CD79B	−0.125 ± 0.061	0.016 ± 0.047	0.002 ± 0.056	2.00×10^{-14}	−0.132	2.81×10^{-11} (Hypo)

(B) Hallmark genes for Cluster II

Target ID[8]	Chrom[9]	Position[10]	Gene symbol	DNA methylation level in non-cancerous lung tissue (N) samples[11] (mean ± SD)			*p*-value of Welch's *t*-test (II *vs.* I and III)[12]	Δβ (II-I and III) [13]	*p*-value of Jonckheere–Terpstra trend test in II[14]
				Cluster I	Cluster II	Cluster III			
cg14074641	16	48,181,753	*ABCC12*	−0.002 ± 0.091	0.025 ± 0.054	−0.109 ± 0.105	1.01×10^{-10}	0.101	7.05×10^{-2} (Hyper)

(C) Hallmark genes for Cluster III

Target ID [15]	Chrom[16]	Position[17]	Gene symbol	DNA methylation level in non-cancerous lung tissue (N) samples[18] (mean ± SD)			*p*-Value of Welch's *t*-test (III *vs.* I and II)[19]	Δβ (III-I and II) [20]	*p*-Value of Jonckheere–Terpstra trend test in III[21]
				Cluster I	Cluster II	Cluster III			
cg26606064	11	125,439,070	*EI24*	0.020 ± 0.083	0.008 ± 0.064	0.115 ± 0.105	8.57×10^{-10}	0.101	2.36×10^{-2} (Hyper)
cg17872476	10	114,205,654	*VTI1A*	−0.034 ± 0.091	−0.035 ± 0.060	−0.137 ± 0.120	1.61×10^{-8}	−0.102	1.51×10^{-2} (Hypo)

Table 3. Genes for which DNA methylation levels were hallmarks for Clusters I, II and III in the learning cohort (Continued)

(C) Hallmark genes for Cluster III

Target ID [15]	Chrom[16]	Position[17]	Gene symbol	DNA methylation level in non-cancerous lung tissue (N) samples[18] (mean ± SD)			*p*-Value of Welch's *t*-test (III *vs.* I and II)[19]	Δβ (III-I and II) [20]	*p*-Value of Jonckheere–Terpstra trend test in III[21]
				Cluster I	Cluster II	Cluster III			
cg21063899	13	78,109,801	*SCEL*	0.033 ± 0.088	0.013 ± 0.054	−0.081 ± 0.086	3.06×10^{-12}	−0.103	1.47×10^{-9} (Hypo)
cg14074641	16	48,181,753	*ABCC12*	−0.002 ± 0.091	0.025 ± 0.054	−0.109 ± 0.105	1.40×10^{-12}	−0.121	2.44×10^{-1} (Hypo)

[1]Probe ID for the Infinium HumanMethylation27 Bead Array.
[2]Chromosome.
[3]National Center for Biotechnology Information (NCBI) Database (Genome Build 37).
[4]$\Delta\beta_{N\text{-}averageC}$.
[5]Average β_{N-C} in Cluster I *versus* average β_{N-C} in Clusters II and III. Such **p** values were calculated to reveal the hallmark genes of Cluster I that showed DNA methylation statuses significantly different in their N samples in comparison with N samples from other clusters (Clusters II and III).
[6]Average β_{N-C} in Cluster I minus average β_{N-C} in Clusters II and III. If Δβ (I-II and III) was more than 0.1, N samples in Cluster I were considered to show DNA hypermethylation relative to N samples in other clusters, and if Δβ (I-II and III) was less than −0.1, N samples in Cluster I were considered to show DNA hypomethylation relative to N samples in other clusters.
[7]Stepwise DNA hypermethylation (Hyper) and hypomethylation (Hypo) from normal lung tissue samples to N samples, and then to tumorous tissue samples in Cluster I.
[8]Probe ID for the Infinium HumanMethylation27 Bead Array.
[9]Chromosome.
[10]National Center for Biotechnology Information (NCBI) Database (Genome Build 37).
[11]$\Delta\beta_{N\text{-}averageC}$.
[12]Average β_{N-C} in Cluster II *versus* average β_{N-C} in Clusters I and III. Such *p* value was calculated to reveal the hallmark gene of Cluster II that showed DNA methylation status significantly different in their N samples in comparison with N samples from other clusters (Clusters I and III).
[13]Average β_{N-C} in Cluster II minus average β_{N-C} in Clusters I and III. If Δβ (II−I and III) was more than 0.1, N samples in Cluster II were considered to show DNA hypermethylation relative to N samples in other clusters.
[14]Stepwise DNA hypermethylation (Hyper) and hypomethylation (Hypo) from normal lung tissue samples to N samples, and then to tumorous tissue samples in Cluster II.
[15]Probe ID for the Infinium HumanMethylation27 Bead Array.
[16]Chromosome.
[17]National Center for Biotechnology Information (NCBI) Database (Genome Build 37).
[18]$\Delta\beta_{N\text{-}averageC}$.
[19]Average β_{N-C} in Cluster III *versus* average β_{N-C} in Clusters I and II. Such *p* values were calculated to reveal the hallmark gene of Cluster III that showed DNA methylation statuses significantly different in their N samples in comparison with N samples from other clusters (Clusters I and II).
[20]Average β_{N-C} in Cluster III minus average β_{N-C} in Clusters I and II. If Δβ (III-I and II) was more than 0.1, N samples in Cluster III were considered to show DNA hypermethylation relative to N samples in other clusters and if Δβ (III-I and II) was less than −0.1, N samples in Cluster III were considered to show DNA hypomethylation relative to N samples in other clusters.
[21]Stepwise DNA hypermethylation (Hyper) and hypomethylation (Hypo) from normal lung tissue samples to N samples, and then to tumorous tissue samples in Cluster III.

Table 4. Correlation between DNA methylation levels of hallmark genes for Clusters I, II and III and the clinicopathological parameters in the validation cohort

(A) Hallmark genes for Cluster I

		DNA methylation level in non-cancerous lung tissue (N) samples[2] (mean ± SD)											
		Pleural anthracosis			Emphysematic change			Atypical adenomatous hyperplasia			Tumor anthracosis		
Target ID [1]	Gene symbol	G1	G2-3	*p*-Value[3]	Negative	Positive	*p*-Value[3]	Absence	Presence	*p*-Value[3]	Negative	Positive	*p*-Value[3]
cg20249919	*PCSK6*	−0.126 ± 0.049	−0.049 ± 0.102	1.83×10^{-2}	−0.069 ± 0.067	−0.049 ± 0.131	4.99×10^{-1}	−0.056 ± 0.101	−0.096 ± 0.082	3.57×10^{-1}	−0.077 ± 0.085	−0.047 ± 0.105	3.18×10^{-1}
cg23349790	*IGSF21*	−0.044 ± 0.101	−0.002 ± 0.100	4.13×10^{-1}	−0.035 ± 0.072	0.028 ± 0.118	3.50×10^{-2}	−0.005 ± 0.101	−0.029 ± 0.086	5.79×10^{-1}	−0.054 ± 0.079	0.017 ± 0.098	1.68×10^{-2}
cg22285621	*SSH3*	−0.073 ± 0.043	0.002 ± 0.101	1.25×10^{-2}	−0.001 ± 0.077	−0.014 ± 0.121	6.52×10^{-1}	−0.004 ± 0.101	−0.035 ± 0.059	3.41×10^{-1}	−0.015 ± 0.077	0.001 ± 0.106	5.69×10^{-1}
cg15433631	*IRX2*	−0.041 ± 0.061	0.034 ± 0.074	4.73×10^{-2}	0.025 ± 0.068	0.029 ± 0.083	8.52×10^{-1}	0.026 ± 0.077	0.028 ± 0.056	9.46×10^{-1}	0.010 ± 0.074	0.037 ± 0.072	2.77×10^{-1}
cg21949305	ADORA2A, CYTSA	0.025 ± 0.091	0.026 ± 0.060	9.73×10^{-1}	0.015 ± 0.054	0.039 ± 0.069	1.91×10^{-1}	0.029 ± 0.063	−0.003 ± 0.036	1.28×10^{-1}	−0.004 ± 0.058	0.039 ± 0.061	3.48×10^{-2}
cg10942056	*DISP1*	0.014 ± 0.088	0.015 ± 0.068	9.71×10^{-1}	0.009 ± 0.062	0.023 ± 0.077	5.00×10^{-1}	0.019 ± 0.071	−0.022 ± 0.027	2.48×10^{-2}	−0.007 ± 0.056	0.026 ± 0.072	1.08×10^{-1}
cg15149645	NUPR1	−0.007 ± 0.124	0.013 ± 0.073	7.37×10^{-1}	0.006 ± 0.070	0.015 ± 0.085	7.06×10^{-1}	0.015 ± 0.079	−0.036 ± 0.022	2.81×10^{-3}	−0.015 ± 0.081	0.021 ± 0.077	1.77×10^{-1}
cg06954481	*GBX2*	−0.044 ± 0.031	0.013 ± 0.075	9.57×10^{-3}	0.008 ± 0.062	0.003 ± 0.085	7.95×10^{-1}	0.012 ± 0.073	−0.047 ± 0.040	2.27×10^{-2}	−0.012 ± 0.058	0.016 ± 0.078	1.90×10^{-1}
cg21250978	*PRKAR2B*	−0.013 ± 0.092	0.002 ± 0.058	7.44×10^{-1}	−0.010 ± 0.050	0.014 ± 0.070	1.95×10^{-1}	0.005 ± 0.061	−0.037 ± 0.033	4.81×10^{-2}	−0.032 ± 0.058	0.013 ± 0.059	2.63×10^{-2}
cg22418909	SFRP1	−0.043 ± 0.076	0.002 ± 0.058	2.55×10^{-1}	0.000 ± 0.065	−0.003 ± 0.053	8.32×10^{-1}	0.003 ± 0.061	−0.041 ± 0.022	4.86×10^{-3}	−0.020 ± 0.057	0.007 ± 0.060	1.64×10^{-1}
cg26200585	*PRX*	0.020 ± 0.079	0.015 ± 0.066	8.81×10^{-1}	0.013 ± 0.069	0.016 ± 0.063	8.89×10^{-1}	0.019 ± 0.067	−0.029 ± 0.035	3.48×10^{-2}	−0.006 ± 0.054	0.025 ± 0.070	1.19×10^{-1}
cg24396745	*HCN4*	−0.056 ± 0.035	0.020 ± 0.072	3.53×10^{-3}	0.017 ± 0.066	0.003 ± 0.079	4.87×10^{-1}	0.015 ± 0.073	−0.025 ± 0.054	1.86×10^{-1}	−0.005 ± 0.074	0.022 ± 0.071	2.60×10^{-1}
cg04330449	*NEUROG1*	−0.040 ± 0.033	0.010 ± 0.073	2.33×10^{-2}	0.010 ± 0.065	−0.005 ± 0.078	4.52×10^{-1}	0.006 ± 0.072	−0.020 ± 0.056	3.82×10^{-1}	−0.006 ± 0.044	0.012 ± 0.078	3.40×10^{-1}
cg19589427	*TNFSF18*	−0.008 ± 0.078	−0.010 ± 0.070	9.65×10^{-1}	−0.010 ± 0.078	−0.012 ± 0.057	9.26×10^{-1}	−0.007 ± 0.071	−0.042 ± 0.036	1.10×10^{-1}	−0.040 ± 0.057	0.005 ± 0.069	3.13×10^{-2}
cg16731240	*ZNF577*	−0.042 ± 0.037	0.014 ± 0.087	2.50×10^{-2}	0.012 ± 0.1000	0.003 ± 0.060	7.02×10^{-1}	0.007 ± 0.086	0.014 ± 0.078	8.48×10^{-1}	−0.015 ± 0.074	0.020 ± 0.087	1.79×10^{-1}
cg03544320	*CRMP1*	−0.097 ± 0.083	0.018 ± 0.094	3.14×10^{-2}	0.010 ± 0.109	−0.005 ± 0.084	5.67×10^{-1}	0.008 ± 0.102	−0.040 ± 0.036	4.56×10^{-2}	−0.014 ± 0.095	0.019 ± 0.097	3.04×10^{-1}
cg12864235	*CDH9*	0.032 ± 0.054	0.027 ± 0.057	8.51×10^{-1}	0.025 ± 0.045	0.030 ± 0.066	7.86×10^{-1}	0.031 ± 0.057	−0.004 ± 0.019	1.29×10^{-2}	0.012 ± 0.043	0.034 ± 0.060	1.77×10^{-1}
cg15898840	IGFBP3	−0.043 ± 0.030	0.001 ± 0.057	2.53×10^{-2}	−0.004 ± 0.052	−0.007 ± 0.061	8.16×10^{-1}	−0.002 ± 0.056	−0.036 ± 0.037	1.14×10^{-1}	−0.003 ± 0.044	−0.002 ± 0.060	9.36×10^{-1}
cg08044694	*BRD4*	−0.067 ± 0.036	−0.020 ± 0.049	3.84×10^{-2}	−0.021 ± 0.046	−0.028 ± 0.053	6.30×10^{-1}	−0.022 ± 0.050	−0.039 ± 0.035	3.55×10^{-1}	−0.041 ± 0.041	−0.017 ± 0.052	1.12×10^{-1}
cg03734874	*TMEM179*	−0.032 ± 0.034	0.023 ± 0.074	1.62×10^{-2}	0.021 ± 0.076	0.015 ± 0.068	7.56×10^{-1}	0.024 ± 0.072	−0.037 ± 0.039	1.89×10^{-2}	−0.008 ± 0.052	0.030 ± 0.075	5.63×10^{-2}
cg10599444	*MMP14*	−0.063 ± 0.026	−0.010 ± 0.060	4.85×10^{-3}	−0.008 ± 0.057	−0.023 ± 0.060	3.87×10^{-1}	−0.013 ± 0.060	−0.027 ± 0.041	5.25×10^{-1}	−0.026 ± 0.047	−0.007 ± 0.059	2.66×10^{-1}
cg24133115	*PDE10A*	−0.020 ± 0.025	0.022 ± 0.060	1.58×10^{-2}	0.014 ± 0.059	0.020 ± 0.057	7.02×10^{-1}	0.018 ± 0.060	0.004 ± 0.027	3.88×10^{-1}	0.009 ± 0.037	0.024 ± 0.063	3.25×10^{-1}
cg12594641	LYPD6	−0.024 ± 0.041	0.036 ± 0.068	2.45×10^{-2}	0.021 ± 0.062	0.036 ± 0.075	4.61×10^{-1}	0.029 ± 0.071	0.013 ± 0.038	4.43×10^{-1}	0.025 ± 0.045	0.035 ± 0.075	5.94×10^{-1}
cg05724065	PHKG1	0.016 ± 0.100	0.011 ± 0.057	9.10×10^{-1}	0.014 ± 0.055	0.008 ± 0.067	7.39×10^{-1}	0.016 ± 0.061	−0.032 ± 0.027	1.05×10^{-2}	−0.002 ± 0.066	0.019 ± 0.059	3.33×10^{-1}
cg19466563	SPARCL1	0.018 ± 0.081	0.012 ± 0.055	8.86×10^{-1}	0.007 ± 0.052	0.021 ± 0.060	3.98×10^{-1}	0.019 ± 0.056	−0.035 ± 0.015	4.46×10^{-5}	−0.015 ± 0.047	0.025 ± 0.057	2.24×10^{-2}
cg24433189	SSTR5	0.024 ± 0.075	0.034 ± 0.060	7.96×10^{-1}	0.031 ± 0.052	0.032 ± 0.071	9.63×10^{-1}	0.035 ± 0.062	−0.003 ± 0.027	2.95×10^{-2}	0.026 ± 0.051	0.036 ± 0.065	5.79×10^{-1}
cg24453664	CD59	−0.057 ± 0.039	0.000 ± 0.053	2.44×10^{-2}	−0.002 ± 0.054	−0.009 ± 0.055	6.40×10^{-1}	−0.004 ± 0.054	−0.021 ± 0.050	5.00×10^{-1}	−0.018 ± 0.050	0.001 ± 0.055	2.53×10^{-1}
cg26609631	GSX1	−0.051 ± 0.058	0.006 ± 0.067	9.21×10^{-2}	0.002 ± 0.066	−0.005 ± 0.069	7.29×10^{-1}	0.004 ± 0.068	−0.050 ± 0.025	3.65×10^{-3}	−0.020 ± 0.054	0.010 ± 0.071	1.35×10^{-1}
cg10604646	RGS5	0.038 ± 0.039	0.033 ± 0.058	8.08×10^{-1}	0.013 ± 0.062	0.056 ± 0.041	5.70×10^{-3}	0.037 ± 0.056	−0.014 ± 0.057	1.16×10^{-1}	−0.006 ± 0.063	0.049 ± 0.047	1.07×10^{-2}
cg03355526	ZNF454	−0.061 ± 0.044	0.001 ± 0.075	2.98×10^{-2}	0.003 ± 0.077	−0.012 ± 0.070	4.81×10^{-1}	0.002 ± 0.074	−0.052 ± 0.053	8.77×10^{-2}	−0.007 ± 0.058	0.000 ± 0.078	7.53×10^{-1}
cg27096144	MSX2	−0.066 ± 0.049	0.001 ± 0.063	3.29×10^{-2}	−0.006 ± 0.057	−0.006 ± 0.072	9.95×10^{-1}	−0.003 ± 0.065	−0.026 ± 0.040	2.94×10^{-1}	−0.023 ± 0.055	0.002 ± 0.068	2.05×10^{-1}
cg15520279	HOXD8	−0.021 ± 0.040	0.016 ± 0.070	1.15×10^{-1}	0.015 ± 0.075	0.009 ± 0.056	7.16×10^{-1}	0.014 ± 0.070	−0.006 ± 0.025	2.05×10^{-1}	−0.010 ± 0.038	0.024 ± 0.075	4.76×10^{-2}

Table 4. Correlation between DNA methylation levels of hallmark genes for Clusters I, II and III and the clinicopathological parameters in the validation cohort (Continued)

(A) Hallmark genes for Cluster I

		DNA methylation level in non-cancerous lung tissue (N) samples[2] (mean ± SD)											
		Pleural anthracosis			Emphysematic change			Atypical adenomatous hyperplasia			Tumor anthracosis		
Target ID [1]	Gene symbol	G1	G2-3	*p*-Value[3]	Negative	Positive	*p*-Value[3]	Absence	Presence	*p*-Value[3]	Negative	Positive	*p*-Value[3]
cg11733245	IL2RA	−0.037 ± 0.042	−0.035 ± 0.051	9.29×10^{-1}	−0.023 ± 0.038	−0.047 ± 0.060	1.10×10^{-1}	−0.035 ± 0.051	−0.013 ± 0.023	1.09×10^{-1}	−0.009 ± 0.035	−0.047 ± 0.050	7.07×10^{-3}
cg22325572	CD53	−0.024 ± 0.083	−0.028 ± 0.058	9.23×10^{-1}	−0.017 ± 0.051	−0.040 ± 0.067	1.90×10^{-1}	−0.029 ± 0.060	−0.008 ± 0.057	4.68×10^{-1}	0.003 ± 0.057	−0.041 ± 0.057	2.96×10^{-2}
cg15691199	CEBPE	−0.029 ± 0.080	−0.018 ± 0.064	7.94×10^{-1}	−0.016 ± 0.050	−0.022 ± 0.079	7.79×10^{-1}	−0.022 ± 0.066	0.015 ± 0.021	1.52×10^{-2}	−0.002 ± 0.061	−0.028 ± 0.067	2.28×10^{-1}
cg16927606	U2AF1L4	−0.012 ± 0.079	−0.004 ± 0.054	8.25×10^{-1}	−0.005 ± 0.048	−0.006 ± 0.065	9.54×10^{-1}	−0.010 ± 0.057	0.032 ± 0.025	1.48×10^{-2}	0.009 ± 0.051	−0.012 ± 0.057	2.31×10^{-1}
cg16240480	EDARADD	−0.040 ± 0.103	−0.047 ± 0.072	8.91×10^{-1}	−0.032 ± 0.071	−0.062 ± 0.075	1.61×10^{-1}	−0.048 ± 0.074	−0.017 ± 0.070	3.86×10^{-1}	0.001 ± 0.049	−0.066 ± 0.076	1.24×10^{-3}
cg05596756	FAM113B	−0.010 ± 0.085	−0.010 ± 0.062	9.92×10^{-1}	0.000 ± 0.052	−0.022 ± 0.073	2.22×10^{-1}	−0.014 ± 0.064	0.026 ± 0.025	2.14×10^{-2}	0.011 ± 0.057	−0.020 ± 0.065	1.30×10^{-1}
cg08040471	C17orf62	0.000 ± 0.073	−0.014 ± 0.066	7.11×10^{-1}	−0.002 ± 0.051	−0.024 ± 0.080	2.80×10^{-1}	−0.015 ± 0.068	0.013 ± 0.029	1.21×10^{-1}	0.019 ± 0.053	−0.027 ± 0.066	2.03×10^{-2}
cg20622019	ADA	−0.021 ± 0.073	−0.033 ± 0.068	7.39×10^{-1}	−0.028 ± 0.069	−0.035 ± 0.066	7.31×10^{-1}	−0.036 ± 0.069	0.008 ± 0.021	6.34×10^{-3}	0.002 ± 0.051	−0.047 ± 0.068	1.14×10^{-2}
cg05109049	EVI2B	−0.057 ± 0.106	−0.041 ± 0.090	7.56×10^{-1}	−0.023 ± 0.093	−0.062 ± 0.084	1.32×10^{-1}	−0.044 ± 0.090	−0.009 ± 0.102	5.07×10^{-1}	−0.002 ± 0.054	−0.058 ± 0.099	1.72×10^{-2}
cg07973967	CD79B	−0.034 ± 0.105	−0.028 ± 0.075	9.16×10^{-1}	−0.017 ± 0.060	−0.042 ± 0.094	2.83×10^{-1}	−0.031 ± 0.080	0.007 ± 0.021	2.06×10^{-2}	−0.007 ± 0.067	−0.039 ± 0.081	1.69×10^{-1}

(B) Hallmark genes for Cluster II and III

		DNA methylation level in non-cancerous lung tissue (N) samples[5] (mean ± SD)									
		Lymphatic invasion			Nodal status				Pathological Tumor-Node-Metastasis stage			
Target ID [4]	Gene symbol	Negative	Positive	*p*-Value[6]	N0	N1	N2-3	*p*-Value[6]	IA-IB	IIA-IIB	IIIA-IV	*p*-Value[6]
cg26606064	*EI24*	0.018 ± 0.098	0.098 ± 0.113	3.01×10^{-2}	0.004 ± 0.098	0.010 ± 0.094	0.118 ± 0.091	1.27×10^{-3}	0.009 ± 0.102	−0.008 ± 0.082	0.118 ± 0.091	1.14×10^{-3}
cg17872476	*VTI1A*	−0.035 ± 0.134	−0.126 ± 0.137	4.32×10^{-2}	−0.023 ± 0.132	0.022 ± 0.127	−0.149 ± 0.121	5.69×10^{-3}	−0.020 ± 0.116	−0.016 ± 0.166	−0.149 ± 0.121	6.70×10^{-3}
cg21063899	*SCEL*	−0.043 ± 0.093	−0.109 ± 0.110	6.08×10^{-2}	−0.024 ± 0.082	−0.024 ± 0.090	−0.141 ± 0.096	2.81×10^{-4}	−0.021 ± 0.089	−0.033 ± 0.062	−0.141 ± 0.096	2.60×10^{-4}
cg14074641	*ABCC12*	−0.017 ± 0.118	−0.083 ± 0.117	8.60×10^{-2}	0.005 ± 0.104	−0.006 ± 0.112	−0.118 ± 0.114	2.09×10^{-3}	0.000 ± 0.111	0.014 ± 0.084	−0.118 ± 0.114	2.00×10^{-3}

[1]Probe ID for the Infinium HumanMethylation27 Bead Array.
[2]$\Delta\beta_{N\text{-}averageC}$.
[3]*p* values (Welch's *t*-test) of <0.05 are underlined.
[4]Probe ID for the Infinium HumanMethylation27 Bead Array.
[5]$\Delta\beta_{N\text{-}averageC}$.
[6]*p* values (Welch's *t*-test) of <0.05 are underlined.

strengthened in, T samples (Table 1). These findings are compatible with the "field cancerization" concept in the lung.[29] In our previous study using the Infinium assay, we proved that DNA methylation alterations in N samples resulted in silencing of tumor-related genes in tumorous tissue.[15] However, the correlation between the results of the Infinium assay in N samples and carcinogenetic factors was not examined in detail.

In this epigenetic clustering of patients with LADCs based on DNA methylation profiles in N samples, many of the patients belonging to Cluster I were heavy smokers. In fact, pleural anthracosis, which mainly reflects the long-term cumulative effects of cigarette smoking, was marked in the lungs of patients belonging to Cluster I. Smoking is known to be a cause of COPD. In fact, many patients in Cluster I actually suffered from obstructive ventilation impairment, and histological findings compatible with emphysema and lung fibrosis were observed in their N samples. Moreover, recurrent inflammation is generally associated with COPD,[30] and histological findings compatible with respiratory bronchiolitis[20,21] were actually observed in the lungs of patients belonging to Cluster I. Inflammation is known to be one of the major causes of DNA methylation alterations in precancerous conditions in various organs, such as chronic hepatitis[16,17] and chronic pancreatitis.[31,32] Taken together, the data suggest that the DNA methylation profiles characterizing Cluster I may be established in lung tissue through the long-term cumulative effects of cigarette smoking *via* chronic inflammation under the conditions of COPD. Unlike the previous study, which revealed aberrant DNA methylation of several tumor-related genes in lung cancers themselves of patients with COPD,[33] this study demonstrated for the first time the presence of distinct DNA methylation profiles related to COPD in N samples, based on genome-wide analysis.

The majority of patients belonging to Cluster II were non-smokers, especially young females. DNA methylation profiles characterizing Cluster II may reflect the carcinogenetic pathway that is unrelated to cigarette smoking. Mutation of the *EGFR* gene is well known to be a driver of LADCs in young female non-smokers, especially in Asia.[34] However, Cluster II included LADCs without *EGFR* gene mutations in non-smokers (data not shown), indicating that DNA methylation profiles in Cluster II were not entirely induced by *EGFR* mutation.

Although many of the patients belonging to Cluster III were smokers, the average number of cigarettes smoked per day × year index was lower in Cluster III than in Cluster I. In fact severe pleural anthracosis was not so frequently evident in the lungs of patients belonging to Cluster III. In addition, the incidence of emphysematous change and fibrosis was lower in the adjacent lung tissue of patients in Cluster III than in that of patients in Cluster I. DNA methylation profiles in Cluster III did not develop from a background of chronic inflammation in COPD, but may have developed rapidly before the long-term effects of cigarette smoking had accumulated in the adjacent lung tissue (possibly through more direct effects of carcinogens related or unrelated to cigarette smoking). However, to evaluate more precisely the effects of smoking on DNA methylation profiles, detailed DNA methylation analysis should be performed using purified epithelial cells, such as those from the airway epithelium.

Distinct DNA methylation profiles seem to be established in the non-cancerous lung during the carcinogenetic pathway *via* inflammation in COPD in heavy smokers (Fig. 2*a*), the carcinogenetic pathway unrelated to cigarette smoking (Fig. 2*b*), and the carcinogenetic pathway that occurs not *via* COPD but possibly *via* more direct effects of carcinogens (Fig. 2*c*). Each pathway may have distinct target genes as hallmarks for Clusters I, II and III (Table 3 and Supporting Information Table S3). Among 120 hallmark genes for Clusters I, II and III, 119 (one exception, *ABCC12*, being shared between Clusters II and III) showed ordered differences of DNA methylation from C to N, and then to T samples of the relevant cluster ($p < 0.05$, Jonckheere–Terpstra trend test, Table 3 and Supporting Information Table S3), indicating that a distinct DNA methylation profile in N samples of each cluster is inherited during progression to Ts.

A proportion of genes described in Table 3 and Supporting Information Table S3 may be simple hallmarks of each cluster (simple target genes of each carcinogenetic pathway). However, at least a proportion of DNA methylation alterations occurring during each carcinogenetic pathway actually result in altered expression of target genes, and may participate in establishment of the clinicopathological characteristics of LADCs in each cluster. The DNA methylation profiles in Cluster I may participate in the generation of locally invasive LADCs, which have a large diameter, a progressed T stage, a high histological grade, frequent pleural invasion and tumor anthracosis. DNA methylation profiles in Cluster II may participate in the generation of clinicopathologically less aggressive LADCs with a favorable outcome. DNA methylation profiles in Cluster III may participate in the generation of the most aggressive LADCs showing frequent lymphatic vessel invasion, blood vessel invasion, a high N stage, a high TNM stage and a poor outcome.

Table 3 includes homeobox genes, such as *IRX2* and *HOXD8*, a gene that has been implicated in cell migration, *SPARCL1*, and genes that have been implicated in apoptosis, such as *RGS5* and *EI24*. *IRX2* is known to participate in early lung development in mouse embryos.[35] *HOXD8* is known to be methylated and/or down-regulated in human malignancies, especially in metastatic, rather than in primary lesions.[36,37] *SPARCL1* is an extracellular matrix glycoprotein known to be correlated with cancer invasion.[38,39] *RGS5* is a member of the family of molecules regulating G protein signaling, and stimulates hypoxia-inducible apoptosis.[40] Positive correlations between *RGS5* expression and both tumor differentiation and a favorable outcome have been reported.[41,42] *EI24* is induced by *p53*, suppresses cell growth and induces apoptosis.[43] Reduced expression associated with DNA methylation of *IRX2, HOXD8, SPARCL1, RGS5* and *EI24* in our cohort of LADCs has been confirmed using expression microarray (data not shown). It is

feasible that these target genes of each carcinogenetic pathway participate in determining the clinicopathological characteristics of LADCs in each cluster.

In the validation cohort, the DNA methylation status of hallmark genes identified in N samples of Cluster I was significantly correlated with pleural anthracosis, which reflects the long-term cumulative effects of smoking, and COPD (pulmonary emphysema) in the adjacent lung and tumor anthracosis, which reflect active cancer–stromal interaction in LADCs. The DNA methylation status of the hallmark gene identified in N samples of Cluster II was significantly correlated with lower aggressiveness (low N stage and low TNM stage) of LADCs in the validation cohort. The DNA methylation status of hallmark genes identified in N samples of Cluster III was significantly correlated with aggressiveness of LADCs, such as lymph vessel invasion, a high N stage and a high TNM stage, in the validation cohort. Thus, correlations between distinct DNA methylation profiles in N samples and both carcinogenetic background factors in the adjacent lung tissue and clinicopathological characteristics of LADCs were confirmed in the validation cohort (Table 4).

Receiver operating characteristic curve (ROC) analysis was performed for N samples in the learning cohort, and the thresholds of the representative hallmark genes described in Table 4 were set so that they were nearest to the top left corner of the ROC. Using these thresholds, the sensitivity, specificity and accuracy for prediction of lymphatic vessel involvement, lymph node metastasis, TNM stage and patient outcome (recurrence and death) were calculated in both the learning and validation cohorts (Supporting Information Table S4). Even though Supporting Information Table S4 suggests that the aggressiveness of tumors developing in the same individual patients and patient outcome may be predictable on the basis of DNA methylation status in N samples, further examinations will be needed to set strict criteria for maximal sensitivity, specificity and accuracy.

Although bulk tissue comprising several cell lineages, for a large number of C, N and T samples, was examined in this study, it would be preferable to examine the DNA methylation status of purified cells. Therefore, the DNA methylation status of the representative gene *CASP8* (Infinium probe ID: cg26799474), included in Table 1B, was compared between cancer cells and normal peripheral airway epithelial cells obtained by microdissection from formalin-fixed, paraffin-embedded tissues of representative patients with LADCs and patients without primary lung cancers, respectively, using pyrosequencing. The DNA methylation levels in T samples (0.279 ± 0.184) were significantly lower than those in C samples (0.689 ± 0.042) by Infinium assay ($p = 3.64 \times 10^{-4}$). Such a significant difference was reproduced upon comparison with microdissected normal airway epithelium: pyrosequencing showed that the DNA methylation levels in microdissected cancer cells (0.273 ± 0.313) were significantly lower than those in microdissected normal airway epithelial cells (0.765 ± 0.104) ($p = 2.74 \times 10^{-3}$).

Differences in DNA methylation levels among different cell lineages, such as epithelial and stromal components, are also an important issue. Cancer cells and their stromal cells, such as cancer-associated fibroblasts, were again collected separately by microdissection from formalin-fixed, paraffin-embedded tissues from representative patients with LADCs. The DNA methylation levels of representative genes described in Table 1B were evaluated quantitatively by pyrosequencing. In one of the examined genes (*CASP8* [Infinium probe ID: cg26799474]), the DNA methylation statuses of cancer cells (0.273 ± 0.313) and stromal cells (0.219 ± 0.094) were almost equal, indicating that both may be affected by carcinogenetic factors. For the other examined gene (*LHX1* [Infinium probe ID: cg22660578]), the DNA methylation statuses of cancer cells (0.096 ± 0.141) and stromal cells (0.538 ± 0.486) differed from each other, probably reflecting differences in susceptibility to the effects of carcinogens, or differences in cell lineage.

In summary, DNA methylation profiles reflecting carcinogenetic background factors, such as smoking, inflammation and COPD, appear to be established in adjacent lung tissue in patients with LADCs. Such DNA methylation profiles in adjacent lung tissue may play a role in determining the aggressiveness of tumors developing in the same individual patients, and thus patient outcome.

Acknowledgement

T. Sato is an awardee of a research resident fellowship from the Foundation for Promotion of Cancer Research in Japan.

References

1. Siegel R, Naishadham D, Jemal A. Cancer statistics, 2013. *CA Cancer J Clin* 2013;63:11–30.
2. Sun S, Schiller JH, Gazdar AF. Lung cancer in never smokers—a different disease. *Nat Rev Cancer* 2007;7:778–90.
3. Baylin SB, Jones PA. A decade of exploring the cancer epigenome—biological and translational implications. *Nat Rev Cancer* 2011;11:726–34.
4. Heller G, Zielinski CC, Zochbauer-Muller S. Lung cancer: from single-gene methylation to methylome profiling. *Cancer Metastasis Rev* 2010;29: 95–107.
5. Arai E, Kanai Y. DNA methylation profiles in precancerous tissue and cancers: carcinogenetic risk estimation and prognostication based on DNA methylation status. *Epigenomics* 2010;2: 467–81.
6. Kanai Y. Genome-wide DNA methylation profiles in precancerous conditions and cancers. *Cancer Sci* 2010;101:36–45.
7. Arai E, Chiku S, Mori T, et al. Single-CpG-resolution methylome analysis identifies clinicopathologically aggressive CpG island methylator phenotype clear cell renal cell carcinomas. *Carcinogenesis* 2012;33:1487–93.
8. Zöchbauer-Müller S, Lam S, Toyooka S, et al. Aberrant methylation of multiple genes in the upper aerodigestive tract epithelium of heavy smokers. *Int J Cancer* 2003;107: 612–6.
9. Eguchi K, Kanai Y, Kobayashi K, et al. DNA hypermethylation at the D17S5 locus in non-small cell lung cancers: its association with smoking history. *Cancer Res* 1997;57: 4913–5.
10. Lamy A, Sesboüé R, Bourguignon J, et al. Aberrant methylation of the CDKN2a/p16INK4a gene promoter region in preinvasive bronchial lesions: a prospective study in high-risk patients without invasive cancer. *Int J Cancer* 2002;100: 189–93.
11. Belinsky SA, Palmisano WA, Gilliland FD, et al. Aberrant promoter methylation in bronchial epithelium and sputum from current and former smokers. *Cancer Res* 2002;62:2370–7.

12. Bibikova M, Le J, Barnes B, et al. Genome-wide DNA methylation profiling using Infinium(R) assay. *Epigenomics* 2009;1:177–200.
13. Selamat SA, Chung BS, Girard L, et al. Genome-scale analysis of DNA methylation in lung adenocarcinoma and integration with mRNA expression. *Genome Res* 2012;22:1197–211.
14. Lockwood WW, Wilson IM, Coe BP, et al. Divergent genomic and epigenomic landscapes of lung cancer subtypes underscore the selection of different oncogenic pathways during tumor development. *PLoS One* 2012;7:e37775.
15. Sato T, Arai E, Kohno T, et al. DNA methylation profiles at precancerous stages associated with recurrence of lung adenocarcinoma. *PLoS One* 2013;8:e59444.
16. Nagashio R, Arai E, Ojima H, et al. Carcinogenetic risk estimation based on quantification of DNA methylation levels in liver tissue at the precancerous stage. *Int J Cancer* 2011;129:1170–9.
17. Arai E, Ushijima S, Gotoh M, et al. Genome-wide DNA methylation profiles in liver tissue at the precancerous stage and in hepatocellular carcinoma. *Int J Cancer* 2009;125:2854–62.
18. Ushijima T, Hattori N. Molecular pathways: involvement of Helicobacter pylori-triggered inflammation in the formation of an epigenetic field defect, and its usefulness as cancer risk and exposure markers. *Clin Cancer Res* 2012;18:923–9.
19. Kanai Y, Hirohashi S. Alterations of DNA methylation associated with abnormalities of DNA methyltransferases in human cancers during transition from a precancerous to a malignant state. *Carcinogenesis* 2007;28:2434–42.
20. Garibaldi BT, Illei P, Danoff SK. Bronchiolitis. *Immunol Allergy Clin North Am* 2012;32:601–19.
21. Travis WD, Colby TV, Koss MN, et al. Obstructive pulmonary disease. In: King DW, ed. Atlas of nontumor pathology. Non-neoplastic disorders of the lower respiratory tract. Washington, DC: American Registry of Pathology, 2002:435–71.
22. Kerr KM. Clinical relevance of the new IASLC/ERS/ATS adenocarcinoma classification. *J Clin Pathol* 2013;66:832–8.
23. Noguchi M, Shimosato Y. The development and progression of adenocarcinoma of the lung. *Cancer Treat Res* 1995;72:131–42.
24. Colby TV, Noguchi M, Henschke C, et al. Adenocarcinoma. In: Travis WD, Brambilla E, Muller-Hermelink HK, Harris CC, eds. World health classification of tumours pathology and genetics of tumours of the lung, pleura, thymus and heart. Lyon: IARC Press, 2004:35–44.
25. Wang D, Minami Y, Shu Y, et al. The implication of background anthracosis in the development and progression of pulmonary adenocarcinoma. *Cancer Sci* 2003;94:707–11.
26. Noguchi M, Morikawa A, Kawasaki M, et al. Small adenocarcinoma of the lung. Histologic characteristics and prognosis. *Cancer* 1995;75:2844–52.
27. UICC International Union Against Cancer. Lung and pleural tumours. In: Sobin LH, Gospodarowicz MK, Wittekind C, eds. TNM classification of malignant tumours, 7th edn. Oxford: Wiley-Blackwell, 2009:138–46.
28. Hu L, Sekine M, Gaina A, et al. Association of smoking behavior and socio-demographic factors, work, lifestyle and mental health of Japanese civil servants. *J Occup Health* 2007;49:443–52.
29. Kadara H, Kabbout M, Wistuba II. Pulmonary adenocarcinoma: a renewed entity in 2011. *Respirology* 2012;17:50–65.
30. Decramer M, Janssens W, Miravitlles M. Chronic obstructive pulmonary disease. *Lancet* 2012;379:1341–51.
31. Peng DF, Kanai Y, Sawada M, et al. DNA methylation of multiple tumor-related genes in association with overexpression of DNA methyltransferase 1 (DNMT1) during multistage carcinogenesis of the pancreas. *Carcinogenesis* 2006;27:1160–8.
32. Peng DF, Kanai Y, Sawada M, et al. Increased DNA methyltransferase 1 (DNMT1) protein expression in precancerous conditions and ductal carcinomas of the pancreas. *Cancer Sci* 2005;96:403–8.
33. Suzuki M, Wada H, Yoshino M, et al. Molecular characterization of chronic obstructive pulmonary disease-related non-small cell lung cancer through aberrant methylation and alterations of EGFR signaling. *Ann Surg Oncol* 2010;17:878–88.
34. Sharma SV, Bell DW, Settleman J, et al. Epidermal growth factor receptor mutations in lung cancer. *Nat Rev Cancer* 2007;7:169–81.
35. Mummenhoff J, Houweling AC, Peters T, et al. Expression of Irx6 during mouse morphogenesis. *Mech Dev* 2001;103:193–5.
36. Leshchenko VV, Kuo PY, Shaknovich R, et al. Genomewide DNA methylation analysis reveals novel targets for drug development in mantle cell lymphoma. *Blood* 2010;116:1025–34.
37. Kanai M, Hamada J, Takada M, et al. Aberrant expressions of HOX genes in colorectal and hepatocellular carcinomas. *Oncol Rep* 2010;23:843–51.
38. Hurley PJ, Marchionni L, Simons BW, et al. Secreted protein, acidic and rich in cysteine-like 1 (SPARCL1) is down regulated in aggressive prostate cancers and is prognostic for poor clinical outcome. *Proc Natl Acad Sci USA* 2012;109:14977–82.
39. Turtoi A, Musmeci D, Naccarato AG, et al. Sparc-like protein 1 is a new marker of human glioma progression. *J Proteome Res* 2012;11:5011–21.
40. Jin Y, An X, Ye Z, et al. RGS5, a hypoxia-inducible apoptotic stimulator in endothelial cells. *J Biol Chem* 2009;284:23436–43.
41. Huang G, Song H, Wang R, et al. The relationship between RGS5 expression and cancer differentiation and metastasis in non-small cell lung cancer. *J Surg Oncol* 2012;105:420–4.
42. Wang JH, Huang WS, Hu CR, et al. Relationship between RGS5 expression and differentiation and angiogenesis of gastric carcinoma. *World J Gastroenterol* 2010;16:5642–6.
43. Zhao X, Ayer RE, Davis SL, et al. Apoptosis factor EI24/PIG8 is a novel endoplasmic reticulum-localized Bcl-2-binding protein which is associated with suppression of breast cancer invasiveness. *Cancer Res* 2005;65:2125–9.

frontiers in
GENETICS

MINI REVIEW ARTICLE
published: 14 February 2014
doi: 10.3389/fgene.2014.00024

Multilayer-omics analyses of human cancers: exploration of biomarkers and drug targets based on the activities of the International Human Epigenome Consortium

Yae Kanai[1,2] * *and Eri Arai*[1,2]

[1] *Division of Molecular Pathology, National Cancer Center Research Institute, Tokyo, Japan*
[2] *Core Research for Evolutional Science and Technology, Japan Science and Technology Agency, Tokyo, Japan*

Edited by:
Yoshimasa Saito, Keio University, Japan

Reviewed by:
Makoto Chuma, Hokkaido University, Japan
Masaaki Takamura, Niigata University Graduate School of Medical and Dental Sciences, Japan

***Correspondence:**
Yae Kanai, Division of Molecular Pathology, National Cancer Center Research Institute, 5-1-1 Tsukiji, Chuo-ku, Tokyo 104-0045, Japan
e-mail: ykanai@ncc.go.jp

Epigenetic alterations consisting mainly of DNA methylation alterations and histone modification alterations are frequently observed in cancers associated with chronic inflammation and/or persistent infection with viruses or other pathogenic microorganisms, or with cigarette smoking. Accumulating evidence suggests that alterations of DNA methylation are involved even in the early and precancerous stages. On the other hand, in patients with cancers, aberrant DNA methylation is frequently associated with tumor aggressiveness and poor patient outcome. Recently, epigenome alterations have been attracting a great deal of attention from researchers who are focusing on not only cancers but also neuronal, immune and metabolic disorders. In order to accurately identify disease-specific epigenome profiles that could be potentially applicable for disease prevention, diagnosis and therapy, strict comparison with standard epigenome profiles of normal tissues is indispensable. However, epigenome mechanisms show heterogeneity among tissues and cell lineages. Therefore, it is not easy to obtain a comprehensive picture of standard epigenome profiles of normal tissues. In 2010, the International Human Epigenome Consortium (IHEC) was established to coordinate the production of reference maps of human epigenomes for key cellular states. In order to gain substantial coverage of the human epigenome, the IHEC has set an ambitious goal to decipher at least 1000 epigenomes within the next 7–10 years. We consider that pathway analysis using genes showing multilayer-omics abnormalities, including genome, epigenome, transcriptome, proteome and metabolome abnormalities, may be useful for elucidating the molecular background of pathogenesis and for exploring possible therapeutic targets for each disease.

Keywords: epigenetics, epigenome, DNA methylation, International Human Epigenome Consortium (IHEC), multilayer/integrated disease omics analyses

MICRO RNAs AND HUMAN DISEASES

The Encyclopedia of DNA Elements (ENCODE) Consortium[1] data have revealed in more detail the high degree of complexity of the mammalian transcriptome: 75% of the genome is transcribed into different types of RNA molecules, e.g., protein-coding, long non-coding, pseudogenes, and small RNA genes (Djebali et al., 2012). RNA molecules show much greater variety than previously suspected. Among such RNA molecules, microRNAs (miRNAs) are non-coding RNAs comprising about 22 nucleotides initially transcribed by RNA polymerase II as primary miRNA (pri-miRNA) molecule precursors that possess a stem loop structure (Jinek and Doudna, 2009). RNase III Drosha acts over pri-mRNAs generating a pre-miRNA containing the hairpin (Jinek and Doudna, 2009). The pre-miRNAs are then exported to the cytoplasm and processed by Dicer into mature miRNAs, which are subsequently translocated into the RNA-induced silencing complex (RISC; Gomes et al., 2013). Each miRNA has multiple tasks, such as transcriptional repression via binding to partially complementary sequences in the 3′-untranslated regions of the target mRNAs and direct mRNA degradation via binding to perfectly complementary sequences (He and Hannon, 2004). Therefore, deregulation of miRNA levels may disturb the expression profiles in cells, thereby playing a key role in induction of diseases, such as cancers, neurodegenerative diseases, and autoimmune diseases.

EPIGENETICS AND miRNAs

Saito et al. revealed that treatment with the DNA demethylating agent 5-aza-2′-deoxycytidine and the histone deacetylase inhibitor 4-phenylbutyric acid induced marked changes in the expression profiles of miRNAs in human cancer cell lines. In particular, DNA hypermethylation and induction of active histone marks in the

Abbreviations: CIMP, CpG island methylator phenotype; COPD, chronic obstructive pulmonary disease; IHEC, International Human Epigenome Consortium; LC, normal lung tissue; LN, non-cancerous lung tissue obtained from patients with lung adenocarcinoma; LT, lung adenocarcinoma tissue; PBAT, post-bisulfite adaptor-tagging; RC, normal renal cortex tissue; RN, non-cancerous renal cortex tissue obtained from patients with clear cell renal cell carcinoma; RT, clear cell renal cell carcinoma tissue.

[1]https://genome.ucsc.edu/ENCODE/

promoter region of miR-127 resulted in decreased and increased expression of miR-127, respectively (Saito et al., 2006). Activation of miR-512-5p by epigenetic treatment induced apoptosis of human gastric cancer cell lines via suppression of the *MCL1* gene (Saito et al., 2009). In the human colon cancer cell line HCT116, disturbance of miRNA expression patterns has been reported after disruption of both *DNA methyltransferase* (*DNMT*) *1* and *DNMT3B* (Lujambio et al., 2007). Findings accumulated to date clearly indicate that expression levels of multiple miRNAs, such as let-7a-3, miR-1, miR-9-1, miR-9-3, miR-34a, mir34a*, mir34b/c, miR-124a, miR-126. miR127, miR-342, and miR-512-5p, are regulated epigenetically (Saito et al., 2013).

On the other hand, the expression of many proteins involved in epigenetics is regulated by miRNAs. For example, miR-152 acts as a tumor suppressor via suppression of *DNMT1* (Huang et al., 2010). The miR-29 family targets *DNMT3A* and *DNMT3B*, whereas miR-101 targets *EZH2* and may alter global chromatin structure (Fabbri et al., 2007). In addition, it has been shown that miRNA has the capacity to recognize chromatin by increasing the methylation of histone, for example through histone H3 lysine 27 tri-methylation (Kim et al., 2008). Thus the close connection between epigenetic alterations and miRNA dysregulation may have a great impact on human diseases.

PARTICIPATION OF EPIGENETIC ALTERATIONS IN MULTISTAGE HUMAN CARCINOGENESIS

Epigenetic alterations, consisting mainly of DNA methylation alterations and histone modification alterations, are often observed in cancers that are associated with chronic inflammation and/or persistent infection with viruses, such as hepatitis B or C viruses, Epstein–Barr virus, and human papillomavirus, or with cigarette smoking (Kanai and Hirohashi, 2007). Accumulating evidence suggests that alterations of DNA methylation are involved even in the early and precancerous stages (Arai and Kanai, 2010). On the other hand, in patients with cancers, aberrant DNA methylation is frequently associated with tumor aggressiveness and poor patient outcome (Kanai, 2008). Precancerous conditions showing alterations of DNA methylation may progress rapidly and generate more malignant cancers (Kanai, 2010).

As we described in the webpage of our laboratory[2], even though genetic alterations, such as activation of oncogenes and inactivation of tumor suppressor genes, have been considered to provide the molecular framework of multistage human carcinogenesis, genetic events alone may not explain the histological heterogeneity underlying the complex biological characteristics of tumors. Therefore, in the 1990s, we began to focus on epigenetic events that can be reversible, in an attempt to explain why cancers show such histopathological heterogeneity. At a time when only two genes, *RB* and *VHL*, were known as tumor suppressor genes silenced by DNA methylation, we showed for the first time that the *CDH1* gene, which encodes the E-cadherin cell adhesion molecule and acts as tumor suppressor, is silenced by DNA methylation around the promoter region in human cancers (Yoshiura et al., 1995). In 1996, we demonstrated that DNA methylation alterations frequently occurred at multiple loci on chromosome 16, one of the hot spots for loss of heterozygosity in liver cancers. This preceded loss of heterozygosity even at the chronic hepatitis or liver cirrhosis stages, which are widely considered to be precancerous conditions. This was one of the earliest reports of aberrant DNA methylation at the precancerous stage (Kanai et al., 1996).

Since then, we have reported DNA methylation alterations in tissue specimens at precancerous stages and in cancers using a candidate-gene approach. As an example of inflammation-associated carcinogenesis, ductal adenocarcinomas of the pancreas frequently develop in a background of chronic pancreatitis. Under these conditions, at least a proportion of peripheral pancreatic duct epithelia may be at the precancerous stage. It has been reported that the average number of methylated tumor-related genes, the incidence of DNA methylation of at least one of such genes, and the expression level of *DNMT1* protein are increased in pancreatic duct epithelia with an inflammatory background, and in another precancerous lesion, pancreatic intraductal neoplasia (PanIN), in comparison with normal pancreatic duct epithelia (Peng et al., 2006).

Urothelial carcinomas of the urinary bladder, renal pelvis, and ureter are clinically remarkable because of their multicentricity and tendency to recur. Such multiplicity may be attributable to the "field effect." Even non-cancerous urothelia showing no marked histological findings from patients with urothelial carcinomas can be considered precancerous, because they may have been exposed to carcinogens in the urine. It has been reported that the average number of methylated tumor-related genes and the expression level of *DNMT1* protein are increased in non-cancerous urothelia showing no marked histological findings from patients with urothelial carcinomas, in comparison with normal urothelia from patients without urothelial carcinomas (Nakagawa et al., 2005). Thus, overexpression of the major DNMT, *DNMT1*, may result in accumulated hypermethylation of DNA for tumor-related genes (Etoh et al., 2004). On the other hand, splicing alteration of *DNMT3B* may induce chromosomal instability through DNA hypomethylation of pericentromeric satellite regions (Saito et al., 2002).

As we described in the webpage of our laboratory[2], after genome-wide epigenetic (epigenome) analysis had become practical, we employed the bacterial artificial chromosome array-based methylated CpG island amplification (BAMCA) method for overviewing the DNA methylation tendency of large individual chromosomal regions. Although precancerous conditions in the kidney have rarely been described, despite the lack of any marked histological findings or association with chronic inflammation or persistent infection with pathogens, it can be considered that non-cancerous renal cortex tissue obtained from patients with renal cancers is already at the precancerous stage showing genome-wide DNA methylation alterations (Arai et al., 2006). We showed that DNA methylation profiles at the precancerous stage are inherited by renal cancers developing in individual patients, and that DNA methylation alterations at the precancerous stage determine both the aggressiveness of subsequently developing cancers and patient outcome through inducing further epigenetic and genetic alterations (Arai et al., 2009a). In addition, we have developed indicators for carcinogenetic risk estimation in patients with chronic hepatitis and liver cirrhosis (Arai et al., 2009b), indicators

[2]http://www.ncc.go.jp/en/nccri/divisions/01path/01path01.html

for estimating the risk of development of urothelial carcinomas that can be determined from urine samples (Nishiyama et al., 2010), diagnostic markers of pancreatic cancer that can be assessed from specimens of pancreatic juice (Gotoh et al., 2011), and indicators for prognostication of kidney, liver, pancreas, and urinary bladder cancers based on DNA methylation profiling. Based on these findings, we have filed patent applications for epigenome diagnosis techniques, and are now attempting to apply them practically.

ACTIVITIES OF THE INTERNATIONAL HUMAN EPIGENOME CONSORTIUM (IHEC)

Recently, epigenome alterations have been attracting a great deal of attention from researchers who are focusing on not only cancers but also neuronal, immune, and metabolic disorders. On the basis of epigenome profiling, attempts are now being made to elucidate the molecular pathogenesis of such diseases and to explore possible biomarkers and drug targets. In order to accurately identify such disease-specific epigenome profiles that could be potentially applicable for disease prevention, diagnosis, and therapy, strict comparison with standard epigenome profiles of normal tissues is indispensable. However, epigenome mechanisms show heterogeneity among tissues and cell lineages. Therefore, it is not easy to obtain a comprehensive picture of standard epigenome profiles of normal tissues. Based on improvements in next-generation sequencing technology, international collaboration will likely help to reveal standard epigenome profiles.

In 2010, the IHEC was established by researchers and founding agencies from Canada, South Korea, the EU, Italy, Germany, Japan, and the USA (Bae, 2013). As described in the webpage of IHEC[3], the primary goal of the IHEC is "to coordinate the production of reference maps of human epigenomes for key cellular states that are relevant to health and diseases." In order to achieve substantial coverage of the human epigenome, the IHEC has set an ambitious goal to decipher at least 1000 epigenomes[3]. To attain this goal, IHEC will use robust techniques to generate (1) high-resolution maps of histone modifications, H3K4me3, H3K9me3, H3K27me3, H3K27ac, H3K4me1, and H3K36me3, (2) high-resolution DNA methylation maps, (3) landmark maps of transcription start sites for all protein-encoding genes, and (4) a comprehensive catalog of non-coding and small RNAs and their patterns of expression[3]. The target cell types being studied by each team in the participating countries are shown on the IHEC website[4].

In Japan, three Japanese IHEC teams[5] including our team are supported by the Core Research for Evolutional Science and Technology division of the Japan Science and Technology Agency. To strengthen the research bases for cancers of digestive organs, including hepatocellular carcinomas and gastric carcinomas, which show high incidences in Japan, we are now performing standard epigenome analyses of normal epithelial cell lineages in digestive organs (**Figure 1**). Target cells of sufficient quality and quantity are being obtained from materials surgically resected from a range of Japanese patients. For example, for liver, we have obtained samples of normal liver tissue distant from sites of liver metastases from primary colon cancers in partial hepatectomy specimens from patients without viral hepatitis, chronic hepatitis, or liver cirrhosis. To isolate hepatocytes, we have performed collagenase perfusion of cannulated branches of the hepatic vein, followed by low-velocity centrifugation. On average, more than 10^7 dispersed cells can be obtained from each case, and immunocytochemistry has confirmed that the hepatocytes are more than 95% pure. In the stomach and colorectum, we initially employ the crypt isolation technique and collagenase digestion. Thereafter, each normal cell lineage is purified by fluorescence activated cell sorting using appropriate antibodies.

Members of our IHEC team have originally developed the post-bisulfite adaptor-tagging method (PBAT), which is an efficient library preparation method for whole-genome bisulfite sequencing (Miura et al., 2012). For the PBAT method, we first perform bisulfite modification followed by adaptor ligation using random priming. The PBAT method minimally requires sub-microgram DNA for mammalian whole-genome bisulfite sequencing without global PCR amplification. A good correlation of the DNA methylation pattern was observed among PBAT, the standard Methyl C-seq methodology developed by Lister et al. (2008), and the Illumina beads chip Infinium assay. The PBAT method is advantageous in that it requires only a small amount of genomic DNA but has good coverage of GC-rich regions, especially in CpG islands and gene-rich chromosomes. We now propose to make the PBAT method one of the standard protocols for IHEC. Under the supervision of the IHEC, we intend to disclose the data we obtain through the National Bioscience Database Center supported by the Japan Science and Technology Agency. Accurate standard epigenome profiles of digestive organ epithelial cells obtained through IHEC activities will be used to explore more useful biomarkers and drug targets of digestive organ cancers.

MULTILAYER/INTEGRATIVE DISEASE OMICS ANALYSES FOR EXPLORATION OF BIOMARKERS AND DRUG TARGETS

Recently big data analysis has impacted various fields of bioscience, especially disease research. It may not be appropriate to perform epigenome analysis including miRNA analysis using clinical samples. Instead, simultaneous multilayer/integrative disease omics analyses would seem more appropriate, including genome, epigenome, transcriptome, proteome, and metabolome analyses for exploration of drug targets. Since 2010, researchers at six National Centers in Japan, i.e., the National Cancer Center, National Cerebral and Cardiovascular Center, National Center for Neurology and Psychiatry, National Center for Global Health and Medicine, National Center for Child Health and Development and National Center for Geriatrics and Gerontology, have been engaged in a research project "Comprehensive exploration of drug targets based on multilayer/integrative disease omics analyses" supported by the Program for Promotion of Fundamental Studies in Health Sciences of the National Institute of Biomedical Innovation (NiBio) (**Figure 2**). This project has been divided among a number of centers specializing in genome, epigenome, transcriptome, proteome, and metabolome analyses of tissue specimens from patients with various diseases that show a high incidence in the Japanese population. Tissue and body fluid

[3]http://ihec-epigenomes.org/about/objectives/

[4]http://ihec-epigenomes.org/research/cell-types/

[5]http://crest-ihec.jp/

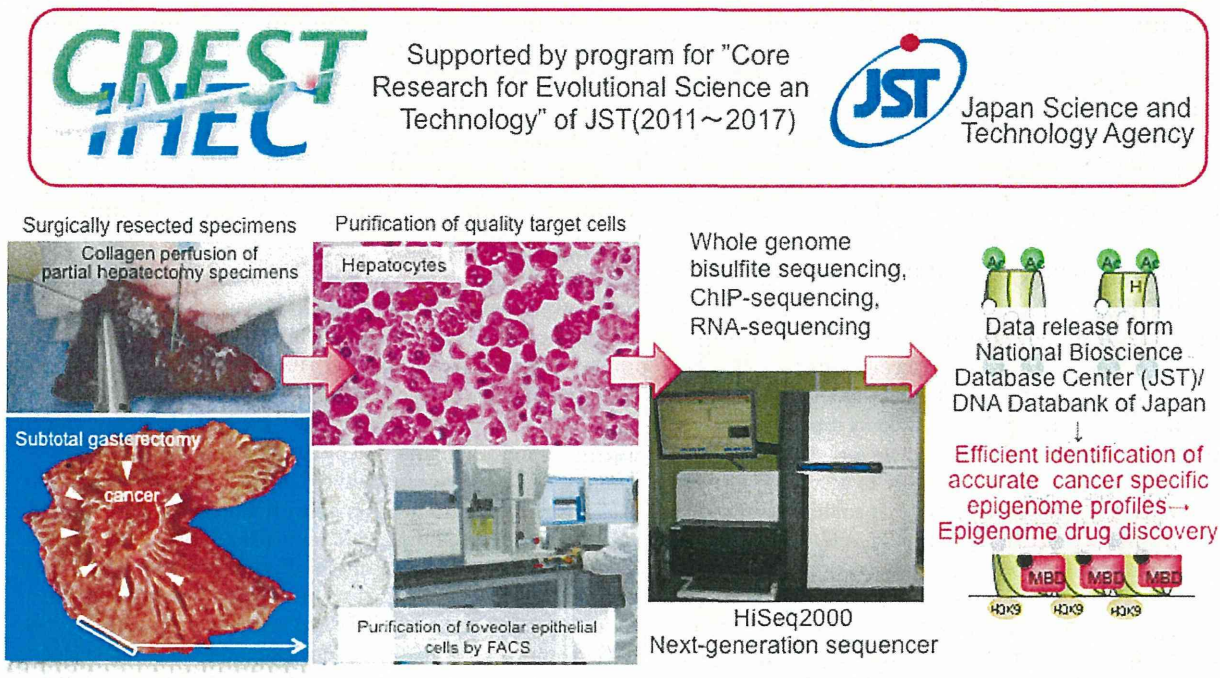

FIGURE 1 | Activity of our team, one of the Japan Teams of the International Human Epigenome Consortium supported by the Core Research for Evolutional Science and Technology division of the Japan Science and Technology Agency (modified from the webpage of our laboratory [http://www.ncc.go.jp/en/nccri/divisions/01path/01path01.html]). We are now performing whole-genome bisulfite sequencing using the post-bisulfite adaptor-tagging method, chromatin immunoprecipitation-sequencing, and RNA-sequencing of purified target cells, i.e., hepatocytes and other live cell lineages, foveolar epithelial cells, and other gastric epithelial cell lineages, and absorptive epithelial cells from the ascending and descending colon and rectum. Accurate epigenome profiling of normal cells will allow the identification of disease-specific epigenome profiles, thus facilitating a potential breakthrough in the prevention, diagnosis, and therapy of diseases.

specimens, cultured cells and animal models of adult cancers, infant leukemia, allergic disease, dilated cardiomyopathy, aortic aneurysm, epilepsy, obesity, non-alcoholic steatohepatitis, spinal canal stenosis, and Alzheimer's disease have been subjected to multilayer-omics analyses. As we described in the webpage of our laboratory[2], we are especially focusing on molecules or molecular pathways which are impaired as a result of multiple mechanisms, such as events in all five omics layers, which may participate in the molecular pathogeneses of diseases and might become potential biomarkers and/or druggable targets (**Figure 2**).

With regard to epigenome analysis of adult cancers in this research project, 414 lung tissue specimens including normal lung tissue (LC) obtained from patients without any primary lung tumor, non-cancerous lung tissue (LN) obtained from patients with lung adenocarcinomas, and lung adenocarcinoma tissue (LT) itself have been subjected to single-CpG resolution Infinium assay. DNA methylation alterations on many probes were evident in LN samples relative to LC samples, and were inherited by, or strengthened in, LT samples. Unsupervised hierarchical clustering using DNA methylation levels in LN samples subclustered patients into clusters I, II, and III. Lung adenocarcinomas in cluster I developed from an inflammatory background in chronic obstructive pulmonary disease (COPD) in heavy smokers, and were locally invasive. Most patients in cluster II were non-smokers and had a favorable outcome. Lung adenocarcinomas in cluster III were most aggressive cancers in light smokers that developed before accumulation of the long-term effects of cigarette smoking, and were probably due to the direct actions of carcinogens, rather than the effects of inflammation. DNA methylation profiles reflecting carcinogenetic factors such as smoking and COPD appear to be established in LNs and may determine the aggressiveness of tumors developing in individual patients, and thus patient outcome (Sato et al., 2014). Among the genes for which DNA methylation status in LN samples was significantly correlated with recurrence of lung adenocarcinomas in individual patients, we focused on *ADCY5, EVX1*, and other genes that were involved in apoptosis and cell adhesion. The mRNA expression levels of these genes were directly regulated by DNA methylation, and a decrease of their mRNA expression in LT samples was significantly correlated with tumor aggressiveness (Sato et al., 2013). When these genes were ectopically expressed in lung cancer cell lines, growth suppression, and apoptosis were induced, indicating that these genes could become therapeutic targets of lung adenocarcinomas.

With regard to epigenome analysis during renal carcinogenesis, 245 renal tissue specimens including normal renal cortex tissue (RC) obtained from patients without any primary renal cancer, non-cancerous renal cortex tissue (RN) obtained from patients with clear cell renal cell carcinomas, and clear cell

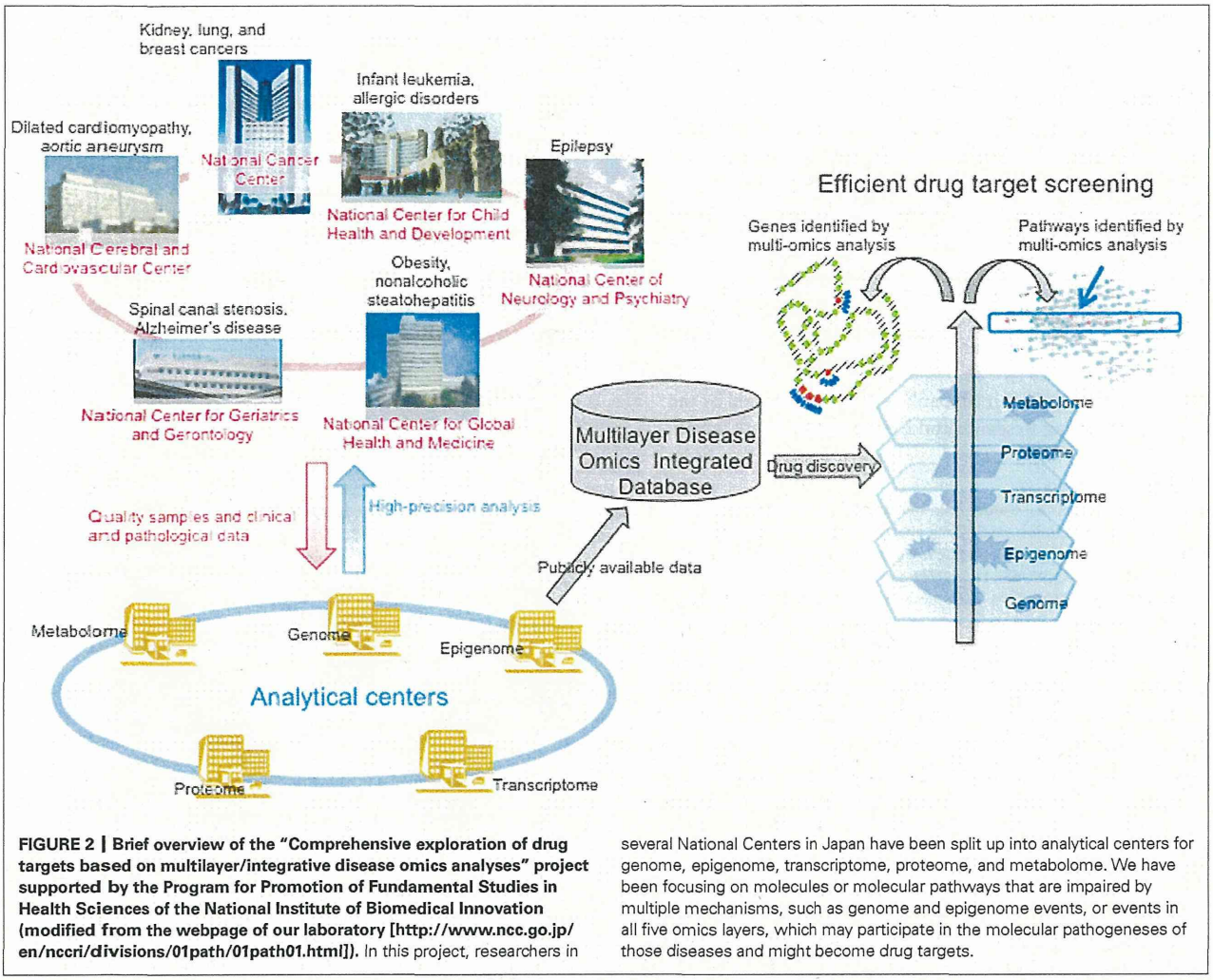

FIGURE 2 | Brief overview of the "Comprehensive exploration of drug targets based on multilayer/integrative disease omics analyses" project supported by the Program for Promotion of Fundamental Studies in Health Sciences of the National Institute of Biomedical Innovation (modified from the webpage of our laboratory [http://www.ncc.go.jp/en/nccri/divisions/01path/01path01.html]). In this project, researchers in several National Centers in Japan have been split up into analytical centers for genome, epigenome, transcriptome, proteome, and metabolome. We have been focusing on molecules or molecular pathways that are impaired by multiple mechanisms, such as genome and epigenome events, or events in all five omics layers, which may participate in the molecular pathogeneses of those diseases and might become drug targets.

renal cell carcinoma tissue (RT) itself were subjected to the Infinium assay. DNA methylation levels at multiple Infinium probe sites were already altered in RN samples relative to RC samples. Unsupervised hierarchical clustering analysis based on DNA methylation levels at the CpG sites where DNA methylation alterations had occurred even in RN samples and were inherited by, and strengthened in, RT samples divided the clear cell renal cell carcinomas into CpG island methylator phenotype (CIMP)-positive and -negative clusters (Arai et al., 2012). Clinicopathologically aggressive cancers were accumulated in the CIMP-positive cluster, where the cancer-free and overall survival rates of the patients were significantly lower than in the CIMP-negative cluster. *FAM150A, GRM6, ZNF540, ZFP42, ZNF154, RIMS4, PCDHAC1, KHDRBS2, ASCL2, KCNQ1, PRAC, WNT3A, TRH, FAM78A, ZNF671, SLC13A5*, and *NKX6-2* have been identified as renal cell carcinoma-specific CIMP marker genes (Arai et al., 2012). Since CIMP-positive renal cell carcinomas show tumor aggressiveness and poorer patient outcome, we established criteria for prognostication of patients with clear cell renal cell carcinomas using renal cell carcinoma-specific CIMP marker genes. We are now performing pathway analysis based on a Bayesian estimation model using multiple genes showing frequent mutations and alterations of expression at the mRNA, miRNA, and protein levels based on multilayer-omics analyses in each of the CIMP-negative and CIMP-positive renal cell carcinomas for exploration of possible drug targets.

PERSPECTIVES

Once DNA methylation alterations occur during multistage carcinogenesis, such alterations are stably preserved on DNA double strands through maintenance methylation mechanisms by *DNMT1*. Therefore, stable stratification of cancers reflecting clinicopathological diversity may be possible based on epigenome profiling. Genes showing epigenome alterations, such as CIMP-marker genes, may become excellent biomarkers discriminating each tumor type stratified on the basis of epigenome profiling. We consider that pathway analysis using genes showing multilayer-omics abnormalities after stratification based on epigenome profiling may be useful for elucidating the molecular background of carcinogenetic pathways